

Attention is all you need for an improved CNN-based flash flood susceptibility modeling. The case of the ungauged Rheraya watershed, Morocco

Akram Elghouat^{a b}, Ahmed Algouti^a, Abdellah Algouti^a, Soukaina Baid^a

^a Cadi Ayyad University, Faculty of Sciences Semlalia, Department of Geology, 2GRNT Laboratory (Geosciences, Geotourism, Natural Hazards and Remote Sensing). Marrakech, Morocco.

^b Interuniversity Institute for Earth System Research (IISTA), University of Granada. 18006, Granada, Spain.

elghouatakram@go.ugr.es , algouti@uca.ac.ma, abalgouti@uca.ac.ma, soukaina.baid@ced.uca.ma

Corresponding Author: elghouatakram@go.ugr.es (A. Elghouat)

Abstract

Effective flood hazard management requires evaluating and predicting flash flood susceptibility. Convolutional neural networks (CNNs) are commonly used for this task but face issues like gradient explosion and overfitting. This study explores the use of an attention mechanism, specifically the convolutional block attention module (CBAM), to enhance CNN models for flash flood susceptibility in the ungauged Rheraya watershed, a flood prone region. We used ResNet18, DenseNet121, and Xception as backbone architectures, integrating CBAM at different locations. Our dataset included 16 conditioning factors and 522 flash flood inventory points. Performance was evaluated using accuracy, precision, recall, F1-score, and the area under the curve (AUC) of the receiver operating characteristic (ROC). Results showed that CBAM significantly improved model performance, with DenseNet121 incorporating CBAM in each convolutional block achieving the best results (accuracy = 0.95, AUC = 0.98). Distance to river and drainage density were identified as key factors. These findings demonstrate the effectiveness of the attention mechanism in improving flash flood susceptibility modeling and offer valuable insights for disaster management.

Keywords: Deep learning, Attention block, Remote sensing, Flash flood susceptibility, CNNs, CBAM

1. Introduction

Flash floods are considered one of the most devastating, costly, challenging, and widespread natural hazards globally (Jeyaseelan 2003, Tingsanchali 2012; Kuenzer et al. 2013; Dahri & Abida 2017; Nogueira et al. 2018; Mohanty et al. 2020). These events emerge from rapid and excessive rainfall occurring within a concise timeframe, typically around 6 hours, and often in mountainous environments (Li et al. 2019), resulting in erosion, landslides, substantial damage to infrastructure and properties, and even significant loss of life (Cao et al. 2016). In fact, they are responsible for almost 84% of global deaths related to natural disaster (Jamali et al. 2020). In recent years, scientific communities worldwide have expressed huge concern about flash floods, as they expect that global warming, population growth, deforestation, and land use planning will increase the frequency and severity of these events, which will result in significant economic and social impacts (Bouwer et al. 2010, De Leijster et al. 2021, Mackay 2008, Woodruff et al. 2013, Hirabayashi et al. 2013, Guha-Sapir et al. 2016, Mekonnen & Hoekstra 2016). Therefore, there is an urgent need for effective spatial prediction of flash flood occurrences on different spatial scales to mitigate their damaging impacts.

Achieving absolute prevention of flood damage seems like a challenging and complex task. Flood management efforts therefore increasingly prioritize proactive measures like evaluating susceptibility and vulnerability in flood-prone regions (Hoque et al. 2019). The comprehensive understanding and identification of these susceptible areas through advanced and appropriate mapping techniques can offer effective mitigation strate-

gies, including emergency evacuation plans (Guerriero et al. 2020; Klipalo et al. 2022; Musolino et al. 2020; Tehrany et al. 2013; Cloke & Pappenberger 2009). Flash flood susceptibility mapping (FFSM) is considered a crucial tool in preventing and managing flash flood events, as it provides significant information about the spatial likelihood of future flash floods taking into consideration topographical features, hydrological aspects, and climatic conditions (Jacinto et al. 2015; Vojtek & Vojteková 2019). This provides targeted guidance to facilitate the implementation of flash flood control and disaster reduction measures that can subsequently reduce potential losses (Choubin et al. 2019; Hong et al. 2018; Saha et al. 2021). Modeling susceptibility to flash floods is thus a prominent global research focus nowadays.

Multiple methods have been developed by researchers to assess and measure flood susceptibility (Sahana et al. 2020; Costache et al. 2020a; Islam et al. 2021; Islam et al. 2021; Pradhan et al. 2023). Former approaches primarily relied on expert knowledge, physical-based models such as HEC-RAS, SWAT, WetSpa (Khalil et al. 2017; Ongdas et al. 2020), and traditional statistical models, encompassing techniques like frequency ratio analysis, discriminant analysis, and generalized linear models (GLMs) (Choubin et al. 2019; Zeng et al. 2021). However, these approaches are time-consuming and require extensive measurement datasets (Costache et al. 2022). Recently, the rapid evolution and advancements of technology in both hardware and software have opened the door to the use of more sophisticated and advanced data-driven models in environmental studies. Particularly, several machine learning (ML) algorithms have gained widespread application, such as artificial neural networks (ANN), support vector machines (SVM), random forests (RF), decision trees (DT), naive bayes (NB), and K-Nearest Neighbors (KNN) (Kabir et al. 2020; Pham et al. 2021; Bui et al. 2020b; Wang et al. 2020a; Eini et al. 2020; Lin et al. 2022; Khoirunisa et al. 2021; Priscillia et al. 2021; Khosravi et al. 2018). These models have showcased superior performance and improved assessment quality compared to traditional methods (Elghouat et al. 2024; Khosravi et al. 2018; Hayashi 2019; Gudiyangada Nachappa & Meena 2020; Zhongping et al. 2020). They analyze topography, hydrological traits, land use, and historical flood occurrences to identify key variables influencing flash floods. Moreover, the availability of remote sensing data has facilitated the application of ML techniques. These data sources provide vital information for mapping flood susceptibility by capturing details about past flood events in addition to different linked factors (Zhao et al. 2020). This will help improve our understanding and prediction of floods, contributing to better flood management and mitigation strategies.

Deep learning methods, a subset of ML algorithms, have been increasingly explored for supervised and unsupervised classification, segmentation, and regression tasks. They prove particularly efficient and beneficial when dealing with large datasets (Wang et al. 2020a; Wang et al. 2020b). Among DL models, deep neural networks (DNNs) and convolutional neural networks (CNNs) take precedence in applications due to their capacity and efficiency to automatically identify crucial features in datasets (Alzubaidi et al. 2021). For flood susceptibility, Bentivoglio et al. (2022) highlighted that CNNs are the most utilized deep learning models across a majority of research papers. They showed superior predictive performance over conventional ML algorithms. For instance, Zhao et al. (2020) conducted an urban flood susceptibility study utilizing RF,

SVM, and CNN methods, with CNN demonstrating the highest performance. Wang et al. (2020a) compared SVM and CNN models for mapping flood susceptibility using different data-input methods, revealing CNN's superior accuracy in the 2D-based input approach. Similarly, Liu et al. (2021) assessed the performance of three hybrid models, including SVM, classification and regression trees (CART), and a CNN, with the latter outperforming the other models. These models consistently exhibit strong performance in flood susceptibility studies. Various CNN architectures, such as LeNet-5, AlexNet, VGGNet, ResNet, InceptionNet, and more, have been developed, each with distinct strengths and weaknesses. However, although these CNN architectures are robust and efficient, they still suffer from drawbacks (Joshi et al. 2019). Deeper CNNs commonly face challenges such as gradient explosion or vanishing (Joshi et al. 2019), whereas wider CNNs may induce overfitting phenomena (Joshi et al. 2019). Therefore, the key is to ensure that CNNs concentrate on learning and emphasizing important information instead of learning non-useful background information.

In this context, attention modules have emerged as a significant enhancement for CNN architectures in multiple tasks, including image classification (Vaswani et al. 2017). Along with attention modules, CBAM (i.e., convolutional block attention module) integrates both channel and spatial attention mechanisms within any CNN, allowing the network to focus not only on critical spatial features but also on important channels within the data (Woo et al. 2018). It is a lightweight module that adds very few extra parameters to a CNN and doesn't burden the computations much. Multiple studies have showcased the ability of this module to direct network focus towards learning only the important things, resulting in enhanced performance of their DL models (Zheng et al. 2022; Ravi & Alazab 2023; Mao et al. 2023; Alirezazadeh et al. 2023). However, the literature shows no studies with a focus on flash flood susceptibility modeling. Adding the attention mechanism could therefore make CNNs better at distinguishing and recognizing patterns in data related to flash floods, leading to more accurate results.

This study aims to assess the effectiveness of attention-based CNNs in predicting flash flood susceptibility. The specific objectives were: (1) to compare the performance of CBAM-based CNNs with baseline models such as ResNet18, DenseNet121, and Xception in predicting flash flood susceptibility and use the most accurate model to create a susceptibility map; and (2) to assess the impact of the CBAM attention module's location within the CNN architecture on flash flood susceptibility predictions. In this study, we selected the ungauged Rheraya watershed, a region with a history of flash flood events, and considered 16 well-chosen conditioning factors that influence flash flooding. The innovations of this study include: (1) it is the first application of attention-based CNNs in flash flood susceptibility; (2) it is the first evaluation of the CBAM attention module's location within the CNN architecture on flash flood susceptibility model performance; and (3) the generation of the first deep learning-based flash flood susceptibility map for the Rheraya watershed, a flood-prone area. The findings of this study will assist authorities and policymakers in mitigating the risks of flash flooding in the area and in devising effective measures to prevent potential losses.

2. Materials and Methods

2.1. Study area

The Rheraya watershed lies in the southern region of Marrakech city, within the Western High Atlas area. Its outlet is defined by the Tahanaout hydrometric station at coordinates 31.3°N, 7.9°E (Figure 1). Key population centers in this region include Asni, Imlil, and Moulay Brahim. Regarded as a significant catchment area in the High Atlas range, the Rheraya covers approximately 224 km², with elevations spanning from 1084 to 4167 meters and steep slopes reaching up to 80°. The region experiences an average annual rainfall of 363 mm, with temperatures ranging typically between 18 and 38 degrees Celsius. Hillslopes within this area are characterized by degraded rangelands with sparse vegetation and rocky terrain, while the valley hosts a narrow stretch of cultivated land on both sides of the river (Boudhar et al. 2007).

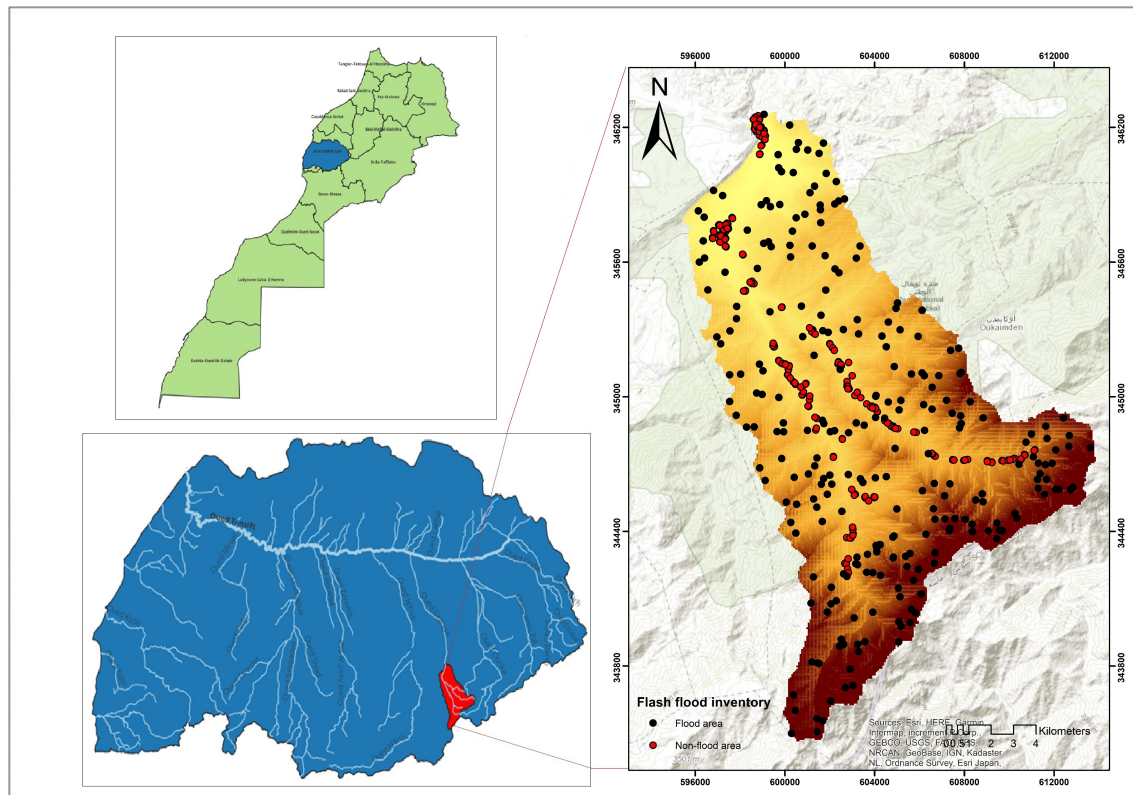


Figure 1: Locations of the study area and historical flash floods

The study area is an ungauged basin with a documented history of destructive flash flood events causing substantial damage to agricultural land, infrastructure, and buildings. Notably, the region experienced a devastating flash flood in 1995 due to intense, short-term rainfall, resulting in over 150 fatalities, including 60 tourists (DIGBY 2000). Additionally, a severe flash flood in 2019 caused significant property damage (Figure 2). The high vulnerability and loss of life in this area are linked to the population's occupation of these exposed regions, primarily for tourism purposes (El Fels et al. 2018). The severity of the consequences of these events and the high frequency of this phenomenon in this region made it suitable for the implementation and

development of an attention-based CNN model for flash flood susceptibility in order to evaluate its efficiency and predictive performance.



Figure 2: Flash flood events and damages in the study area

2.2. Flash flood inventory

Identifying and creating a precise historical inventory of flash floods is an essential step in assessing and investigating the relationship between flash floods and their causal factors, enabling the development of accurate flash flood susceptibility maps (Choubin et al. 2019). Current approaches rely on historical archives, field surveys, and remote sensing satellite data. In this study, we generated an inventory of historical flash flood events based on records from the Hydraulic Basin Agency of Tensift (ABHT), followed by a field survey in which local residents contributed to the development of this inventory. Validating the obtained data is a mandatory step to ensure its trustworthiness and accuracy. Therefore, pre-flood and post-flood remote-sensing images were analyzed to ascertain the existence and validation of the documented flash flood records. We calculated the Sentinel-1 dual-polarization water index (SDWI) and the normalized difference water index (NDWI) using Landsat data to identify the flooded areas (DeVries et al. 2020; Mehmood et al. 2021). The validation step was conducted using the Google Earth Engine platform (GEE).

A total of 261 flash flood locations from 1994 to 2022 were identified. Additionally, we generated 261 points designated as 'non-flash flood' from areas where there was no evidence of flash flood occurrences using the geo-processing tool 'create random points', within the data management tool in ArcGIS software (ESRI 2011).

2.3. Flash conditioning factors

The process of identifying flash flood causative factors lacks a universal framework, as it depends on the complex interactions between local environmental dynamics and historical flash flood events (Gui et al. 2023). Also, these phenomena have characteristics that differ from region to region. Therefore, selecting the most sensitive flash flood conditioning factors is critical for developing an accurate flash flood-susceptibility map. In this study, 16 conditioning factors were thoughtfully selected based on a comprehensive literature review of previous studies, data availability, and the characteristics of flash flood development in the Rheraya watershed (Figure 3,4,5). We made sure to consider different aspects of the study area, including topographical, hydrological, meteorological, environmental, and anthropogenic features (Table 1). All factors were transformed into raster format, then aligned and resampled to 12.5 meters to ensure spatial consistency. Subsequently, data standardization was implemented to ensure a consistent scale and distribution of data values. Finally, the entire dataset was divided into training, validation, and testing sets.

Table 1: Description of the selected conditioning variables

Variables	Data source	Spatial resolution
Topographical factors		
Elevation		12.5 m
Slope		12.5 m
Aspect		12.5 m
Curvature		12.5 m
Distance to river		12.5 m
Topographical positioning index (TPI)		12.5 m
Ruggedness index	Digital Elevation Model (ALOS DEM)	12.5 m
Hydrological and meteorological factors		
Stream power index (SPI)		12.5 m
Topographic wetness index (TWI)		12.5 m
Drainage density		12.5 m
Convergence index		12.5 m
Flow accumulation		12.5 m
Rainfall	Hydraulic Basin Agency of Tensift (ABHT)	-
Environmental and anthropogenic factors		
NDVI	Sentinel-2 MSI - Level-2A Product	10 m
Landcover	ESA WorldCover 2021	10 m
Distance to roads	OpenStreetMap (OSM)	-

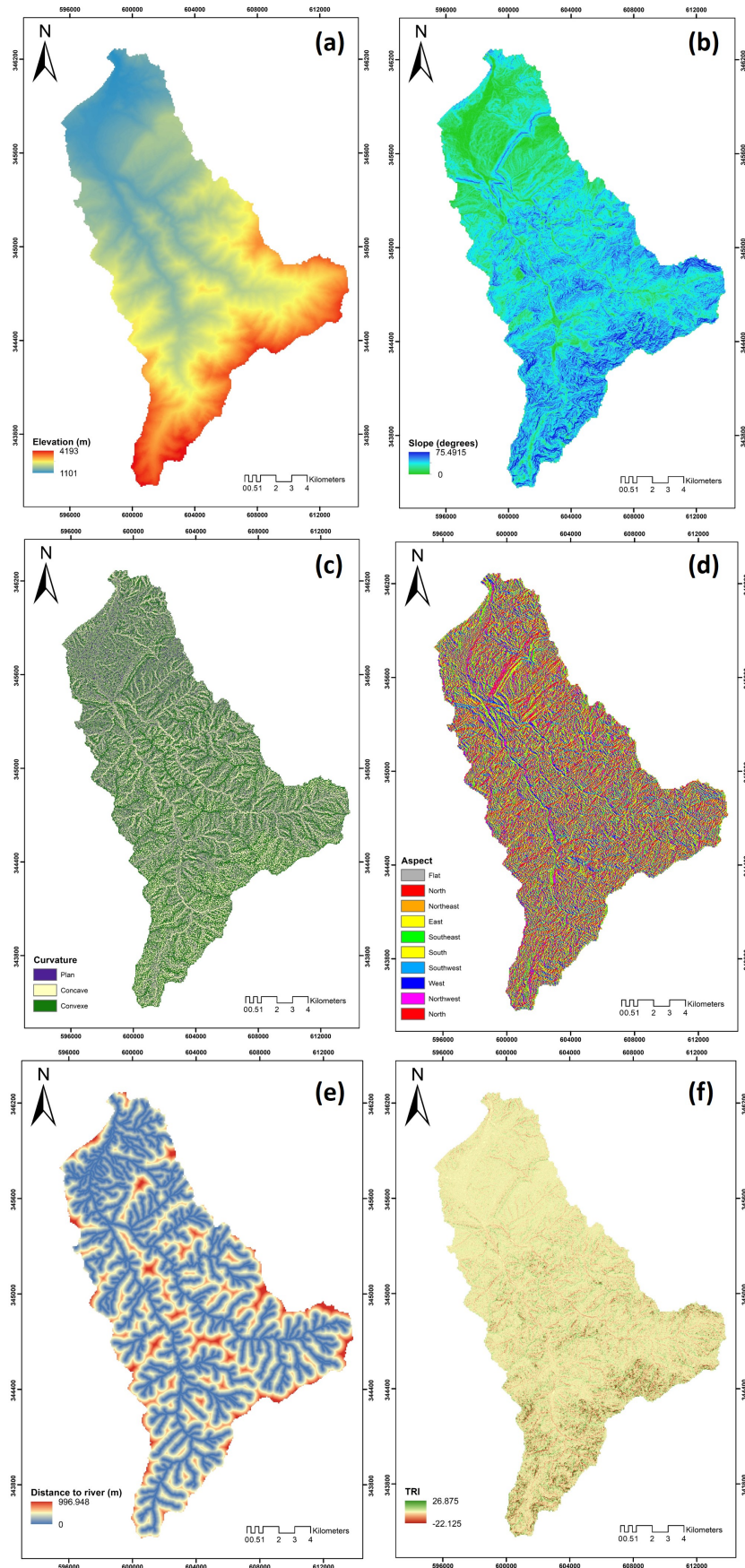


Figure 3: (a) Elevation, (b) slope angle, (c) Curvature, (d) Aspect, (e) Distance to river, (f) TRI

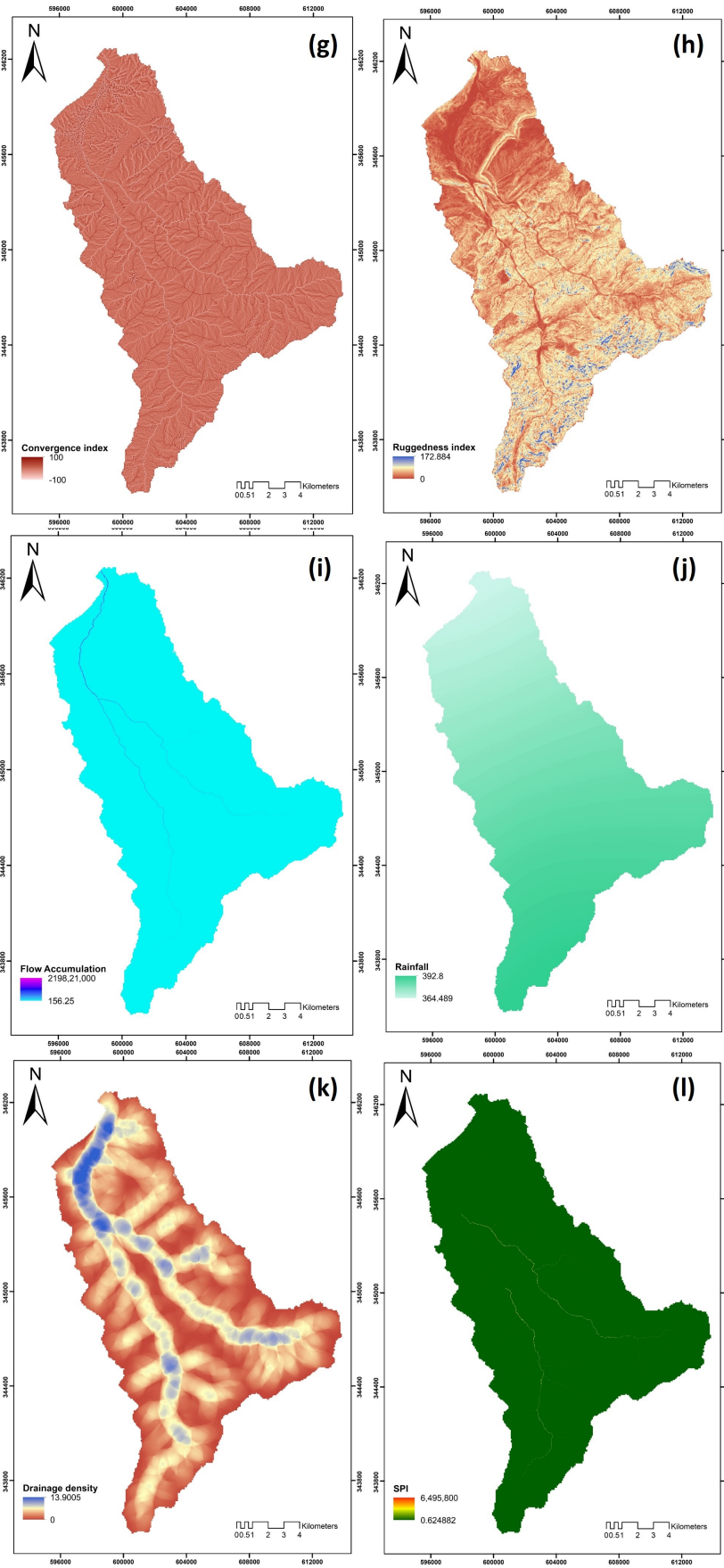


Figure 4: (g) Convergence index, (h) Ruggedness index, (i) Flow accumulation, (j) Rainfall, (k) Drainage density, (l) SPI

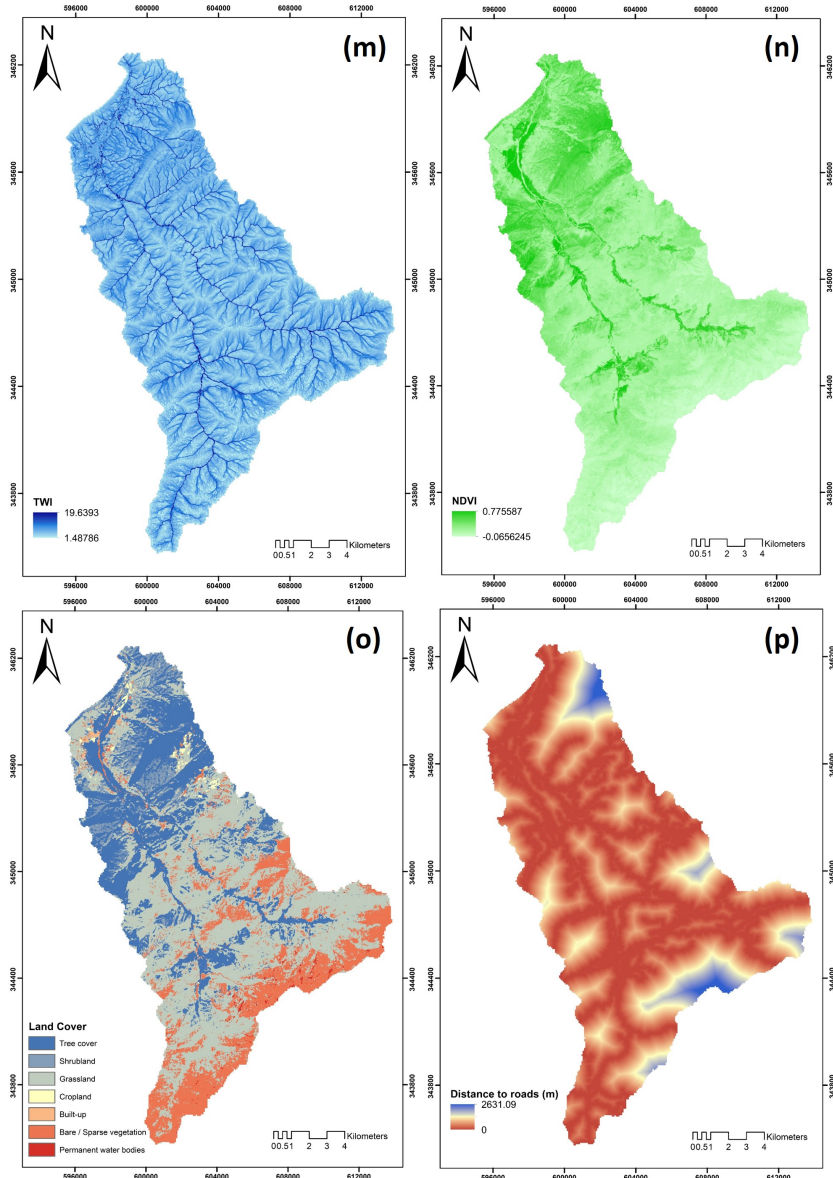


Figure 5: (m) TWI, (n) NDVI, (o) Land cover, (p) Distance to roads

2.3.1. Topographical factors

The topographical factors, including elevation, slope, aspect, curvature, distance to river, convergence index (CI), topographical positioning index (TPI), and ruggedness index (RI), were computed via processing in ArcGIS 10.2. The derived data were obtained using a 12.5 m-resolution PALSAR Phased Array type L-band Digital Elevation Model (DEM) obtained from the Alaska Satellite Facility (ASF). Elevation is a key factor in flash flood modeling, given the inverse relationship between elevation and flash floods (Fernández & Lutz 2010; (Bui et al. 2020b; (Dodangh et al. 2020)). With decreasing elevation, the terrain tends to flatten, leading to increased river water flow and vice versa (Cao et al. 2016). Slope is a critical factor that affects flash floods occurrence, since it affects the speed of the water flow (Stevaux et al. 2020). Regions

with gentler slopes are more likely to accumulate water, potentially facilitating higher infiltration rates and reduced surface runoff speeds. These areas could be more prone to flash floods. Aspect refers to the direction of the predominant slope on the surface of the terrain. It indirectly affects flash flooding as it influences floodwater flow directions, which helps to maintain soil moisture (Chu et al. 2020). Curvature delineates areas where runoff diverges or converges, impacting water flow dynamics (Ginesta Torcivia & Ríos López 2020). Runoff speed can vary based on the slope. Convex slopes often promote faster overland flow, potentially affecting infiltration and soil saturation (Cao et al. 2016), whereas concave slopes might slow down overland flow and potentially aid infiltration (Young & Mutchler 1969). Distance to river significantly influences flash flood vulnerability within a watershed as it affects the extent of flooding (Tehrany et al. 2015). Areas close to the hydrographic network often face a higher susceptibility to flooding compared to those situated farther away (Butler et al. 2006; Chapi et al. 2017). The topographic position index (TPI) measures the elevation difference between a specific point and its surrounding area. It helps identify topographic features like valleys, hills, or bottoms (Zwoliński & Stefańska 2015; Newman et al. 2018). Generally, areas with higher elevations and steeper slope, indicated by TPI, tend to be less susceptible to flash flooding compared to lower-lying regions (Alam et al. 2021). The ruggedness index measures terrain roughness based on elevation variations. In flash floods, rugged terrain might affect water flow patterns, potentially influencing flash flood behavior due to altered landscape topography (Alam et al. 2021).

2.3.2. Hydrological and meteorological factors

Hydrological and meteorological factors directly influence the occurrence and severity of flash floods. Various factors were taken into consideration in this study, such as stream power index (SPI), topographical wetness index (TWI), drainage density, convergence index, flow accumulation, and rainfall. SPI quantifies a river's erosive potential by assessing its ability to transport sediment and erode its bed during flood events, influencing the river's overall fluvial system (Knighton 1999; Pamučar et al. 2017). TWI identifies variations in spatial wetness and highlights areas susceptible to water accumulation (Chapi et al. 2017; Beven & Kirkby 1979; Moore et al. 1991). It helps predict potential flash flood-prone zones by considering the ratios of basin area to slope angles (Wilson & Gallant 2000; Nhu et al. 2020). Drainage density measures the total length of streams within a watershed area (Elmore et al. 2013; Nguyen et al. 2020). Higher drainage densities suggest increased surface runoff potential, which can contribute to flooding under certain conditions (Chapi et al. 2017). The convergence index measures the degree of river network convergence within a region, highlighting valleys and inter-alluvial surfaces (Costache & Zaharia 2017). Flow accumulation quantifies the cumulative flow contribution from neighboring cells towards each specific cell within a terrain. It is a crucial factor in identifying water accumulation patterns and potential flash flood-prone areas in a landscape (Abdel Hamid et al. 2020). Rainfall is one of the most critical factors that causes flash floods (Pourghasemi et al. 2020). These sudden floods arise when rainfall exceeds the ground's capacity to absorb water, causing rapid and unexpected flooding. In this study, we used data from 1994 to 2022 collected from two specific meteorological stations, i.e., Tahanaout and Armed, obtained from the hydraulic basin agency of Tensift (ABHT). The IDW

(i.e., inverse distance weighted) interpolation method was then used to compute the precipitation variable using ArcGIS 10.2 software.

2.3.3. Environmental and anthropogenic factors

Environmental and anthropogenic factors included the NDVI (normalized difference vegetation index), landcover, and distance to roads. The NDVI is an index that reflects the changes in vegetation and surface water cover over time (Ahmed & Akter 2017). It expresses the density of vegetation in a region and has a strong influence on flash flooding (Kumar & Acharya 2016). Areas with lower vegetation cover often exhibit increased vulnerability to flooding (Ngo et al. 2018). In this study, the NDVI was calculated using Sentinel-2 Level-2A data spanning six years, from January 1, 2017, to December 31, 2022, which included a total of 538 Sentinel-2 images. These images were filtered to include only the ones with a cloud cover of 20% or less. Through Google Earth Engine (GEE), we generated a raster representing the mean NDVI across all these years. Land cover has a significant influence on surface runoff, infiltration, evaporation, and sediment transport (Benito et al. 2010; Karlsson et al. 2017; Khosravi et al. 2018). It directly affects flash flood occurrence and frequency, which aids in identifying highly susceptible areas. Urban areas characterized by impermeable surfaces, for instance, are more likely to be flooded compared to areas covered by farmlands, forests, and green vegetation (Rahmati et al. 2016). We used the European Space Agency (ESA) WorldCover product, which provides a global land cover map for 2021 at 10 m resolution based on Sentinel-1 and Sentinel-2 data (Zanaga et al. 2022). The landcover categories included 7 classes, including tree cover, shrubland, grassland, cropland, built-up, bare or sparse vegetation, and permanent water bodies. Distance from roads can significantly impact flooding and the susceptibility of an area to flood risks. Roads often act as barriers, altering natural drainage patterns and increasing surface runoff, elevating flash flood vulnerability. Therefore, distance to roads could be an important variable of flash flood susceptibility (Nachappa et al. 2020). We extracted road data from Open Street Map (OSM), and then we calculated the distance from each pixel to the road feature using the Euclidean distance in ArcGIS 10.2.

2.4. Methodology

In the present research, a CBAM-based CNN model was developed to assess flash flood susceptibility in the Rheraya watershed. Given their advantages, three representative deep CNNs, namely, ResNet 18 (He et al. 2016), Xception (Chollet 2017), and DenseNet121 (Huang et al. 2017), were used as the backbone architectures (detailed in Section 2.4.2). To investigate the impact of the CBAM block on flash flood susceptibility outcomes, we integrated the CBAM at various points within these CNN architectures. Specifically, we tested three insertion points: plugging CBAM into each block of the backbone architecture (Figure 7c), at the head of the backbone architecture (Figure 7a), and at the tail of the backbone architecture (Figure 7b).

The workflow of the study is presented as a flowchart in Figure 6, consisting of five main steps: (1) compilation of the GIS and remote sensing database, including flash flood inventory data and 16 well-

selected flash flood conditioning variables; (2) identification and removal of redundant flash flood influencing variables through factor optimization (i.e., Pearson’s correlation and multi-collinearity analysis), followed by the splitting of the database into training, validation, and testing datasets; (3) developed and trained multiple CBAM-based CNNs, including the attention block at different locations within the architectures, and then evaluated and compared their performance using various statistical metrics. (4) generated a flash flood susceptibility map based on the most robust model; and (5) conducted sensitivity analysis on various flash floods with respect to the influencing variables.

All models were trained using Keras 2.15.0, with TensorFlow 2.15 serving as the backend. Model weights and biases were initialized from scratch, and the network was trained with a batch size of 4. The initial learning rate was set to 0.001, decreasing by a factor of 10 whenever the validation set’s accuracy showed no improvement for 10 consecutive epochs. Models with the lowest validation loss were chosen. Binary cross-entropy served as the loss function for the CNNs. All the analysis and model implementations were performed in Python 3.11.2.

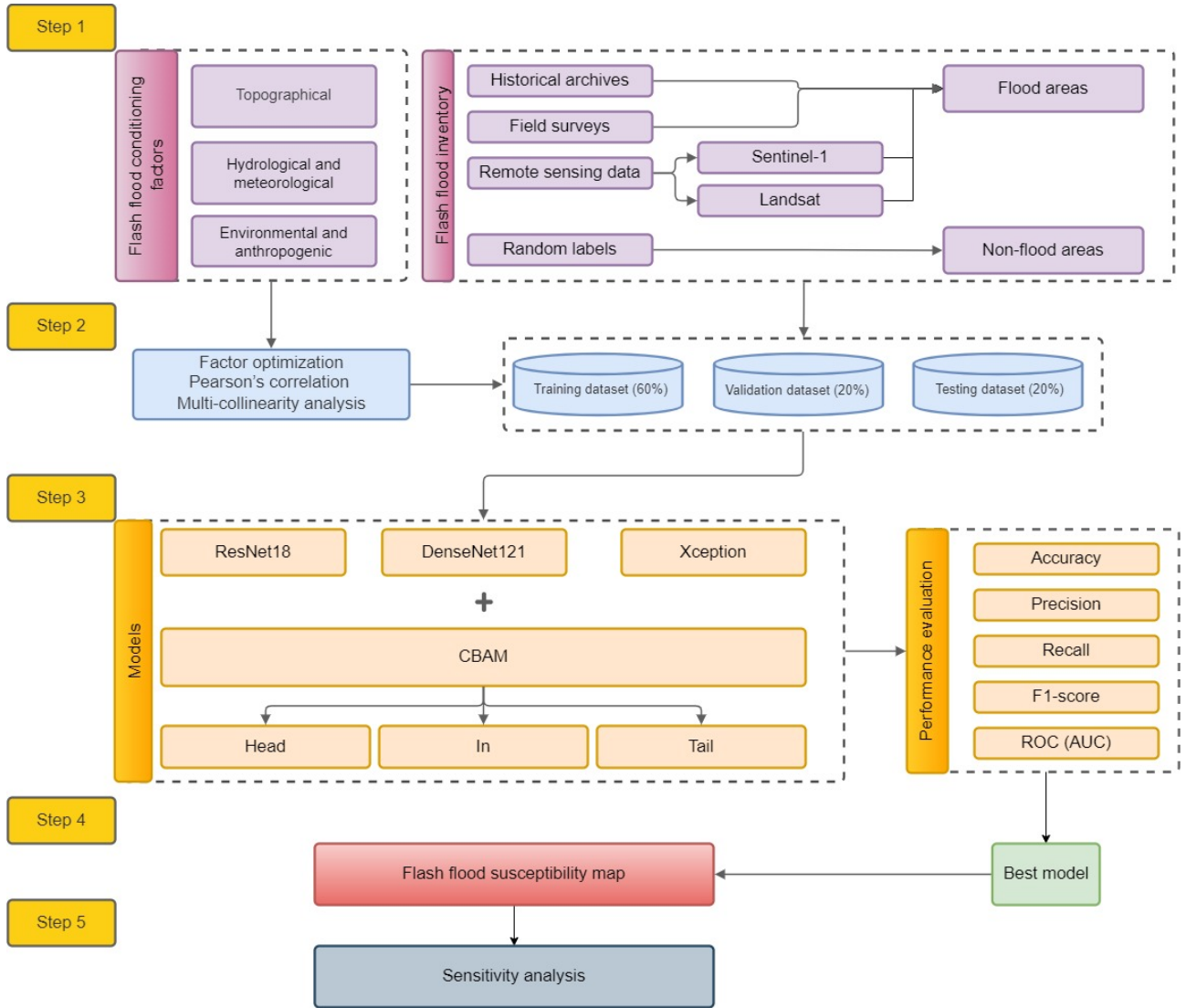


Figure 6: Flowchart of the used methodology

2.4.1. Factor optimization

Identifying and filtering redundant flash flood-influencing factors with limited classification ability enhances the accuracy of the process as it overcomes training challenges related to high data dimensionality (Pham et al. 2021). In the context of classification or regression problems, it is crucial that independent variables exhibit minimal correlation. This increases the prediction power of the models by selecting the most significant factors and removing the irrelevant ones. Therefore, it is crucial to ensure the dependency between the flash flood conditioning variables through correlation and multicollinearity tests. In this study, we initially computed the Pearson correlation coefficient to examine correlations, followed by computing the variance inflation factor (VIF) to assess multicollinearity. These commonly used metrics have demonstrated high efficiency and accuracy in selecting relevant variables in flood susceptibility analysis (Yang et al. 2022; Tsangaratos et al. 2023). The Pearson correlation coefficient quantifies the linear correlation between two

datasets, serving as a tool to evaluate how changes in one variable align with changes in another. It has values ranging from -1 to 1, where a strong correlation is indicated by values equal to or greater than 0.7, a significant correlation falls between 0.5 and 0.7, a weak correlation is between 0.3 and 0.5, and no correlation is indicated when values are lower than 0.3 (Sedgwick 2012). VIF measures multicollinearity among the independent variables, where values higher than 5 to 10 suggest a problem with multicollinearity (Kim 2019).

2.4.2. Models

(a) **ResNet18**

ResNet (Deep residual network) is one of the models developed by He et al. (2016) that addresses challenges encountered in the training of deep neural networks. Training deep learning models is often time-consuming and constrained by the number of layers. To overcome these issues, ResNet incorporates skip connections or shortcuts. Notably, the ResNet model exhibits superior performance compared to alternative architectures, as its effectiveness does not diminish with increasing depth. This results in more efficient computational calculations and improved network training capabilities. The ResNet architecture employs skip connections across two to three layers, incorporating Rectified Linear Unit (ReLU) and batch normalization. He et al. (2016) demonstrated that ResNet excels in image classification, outperforming other models and highlighting its proficiency in extracting image features. The implementation of residual learning across multiple layers is a key aspect of ResNet’s success. The residual block in ResNet is defined as:

$$y = F(x, W + x) \tag{1}$$

where x is the input layer, y is the output layer, and F represents the residual map. ResNet’s residual block is effective when input and output data dimensions are identical. Additionally, each ResNet block comprises either two layers (for ResNet-18 and ResNet-34 networks) or three layers (for ResNet-50 and ResNet-101 networks). The initial two layers of the ResNet architecture resemble GoogleNet, employing a 7×7 convolution and 3×3 max-pooling with a stride of 227. In this study, we chose ResNet-18, which contains 17 convolution layers and 1 fully connected layer.

(b) **DenseNet121**

Dense convolutional networks (DenseNets), introduced by Huang et al. (2017), represent a highly effective architecture alternative to ResNets, showcasing superior performance across various classification tasks, including those in remote sensing applications (Zhang et al. 2019; Tong et al. 2020; Chen & Tsou 2021). In contrast to ResNets, DenseNets feature dense blocks where each layer connects to every preceding layer, incorporating an additional (channel-wise) concatenated input of the previously learned feature maps. This design fosters extensive feature reuse throughout the network, resulting in well-performing and more compact models with fewer trainable parameters compared to an equivalent-sized

ResNet. However, this advantage comes with the trade-off of increased memory requirements during training. Equation 2 defines the operation of Densenet:

$$H(x) = T_k(H_{k-1}(H_{k-2}(\dots H_1(T_0(x))\dots))) \quad (2)$$

Where x is the input to the entire DenseNet; T_0, T_1, \dots, T_k represent the transition layers; H_1, H_2, \dots, H_{k-1} represent the dense blocks; and $H(x)$ is the output of the DenseNet.

Among the numerous DenseNet models, in this study, DenseNet121 was used, where 121 is the total number of layers present in the architecture. DenseNet121 is a deep model comprised of four dense blocks, with the layers between consecutive blocks referred to as transition layers. These transition layers play a crucial role in altering feature-map sizes through convolution and pooling operations.

(c) **Xception**

Xception, proposed by Chollet (2017), is a convolutional neural network architecture that aims to enhance traditional convolutional layers by leveraging depthwise separable convolution layers. The term Xception, short for "Extreme Inception," reflects its inspiration from the Inception architecture. The Xception architecture has 36 convolutional layers, forming the feature extraction base of the network. Unlike standard convolutions, Xception utilizes depthwise separable convolutions, consisting of two steps: depthwise convolutions, where a separate 3x3 convolution is applied for each channel, capturing spatial dependencies; and pointwise convolutions, employing a 1x1 convolution across all channels to mix information. This design optimizes parameter usage, reducing computational costs while preserving expressive power. The architecture is modular, featuring repeated depthwise separable convolution blocks with skip connections to facilitate information flow across different depths. These skip connections aid in training very deep networks and support gradient flow during backpropagation, making Xception efficient and powerful for various deep learning tasks.

(d) **Convolutional block attention module (CBAM)**

Convolutional block attention module (CBAM) is an attention module for convolutional neural networks (Woo et al. 2018). It can be integrated into any CNN to enhance its representational capacity by guiding the model to focus on relevant features and ignore non-useful background information. The architectural overview of CBAM is depicted in Figure 8a. CBAM combines channel and spatial information through convolution operations, emphasizing key features in the convolution layers. This is achieved with two sequential sub-modules: the channel attention module and the spatial attention module, as shown in Figure 8b. Below, we describe the details of each sub-module:

Channel attention module: in the convolution process, each channel of intermediate features is treated as a feature detector. The channel attention module exploits inter-channel relationships to determine the importance of each channel. Initially, the spatial dimension of intermediate features undergoes

average-pooling and max-pooling to generate two distinct context features. Subsequently, these features are transformed by a shared multi-layer perceptron (MLP) and combined through element-wise summation. The resulting fused feature is activated by a sigmoid function, representing the channel importance of the original feature map. Mathematically, the channel attention module's calculation process is defined as:

$$M_c(F) = f_{\text{sigmoid}}(\text{MLP}(\text{AvgPool}(F)) + \text{MLP}(\text{MaxPool}(F))) \quad (3)$$

Spatial attention module: in contrast to the channel attention module, the spatial attention module focuses on determining "where" in the input space significant information lies, complementing the channel attention. It aims to generate refined features by exploiting inter-spatial relations in the original features. This involves applying average-pooling and max-pooling along the channel axis, concatenating the outputs, and converting the concatenated descriptor into a spatial attention map through a 7×7 convolution and a sigmoid operation. The spatial attention module's computation can be expressed as:

$$M_s(F) = f_{\text{sigmoid}}(\text{Conv}([\text{AvgPool}(F); \text{MaxPool}(F)])) \quad (4)$$

Finally, CBAM combines attention maps derived from the channel and spatial attention modules to generate refined feature maps. The combination of the two sub-modules is described by:

$$F' = M_c(F) \otimes F \quad (5)$$

$$F'' = M_s(F') \otimes F' \quad (6)$$

where F represents an intermediate feature map of the CNN, \otimes denotes element-wise multiplication, and F'' is the resulting refined feature map.

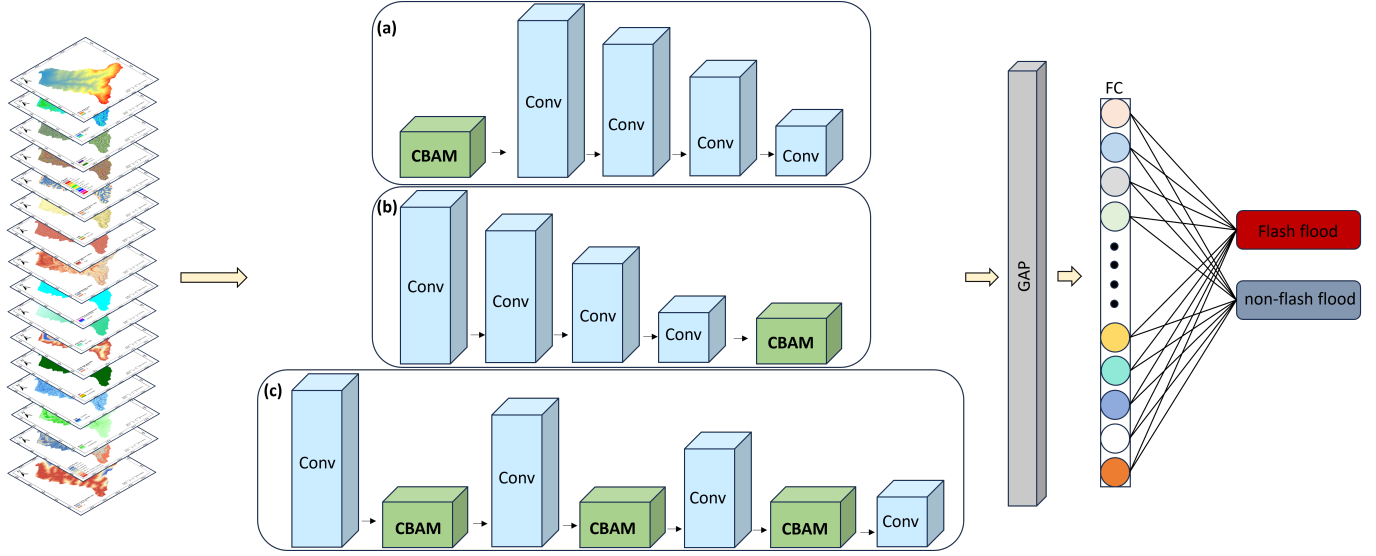


Figure 7: Illustration of the CBAM-based CNN architecture, including the attention module heading the architecture (a), tailing the architecture (b), and plugged in each convolutional block (c). GAP: global average pooling, FC: fully connected layers.

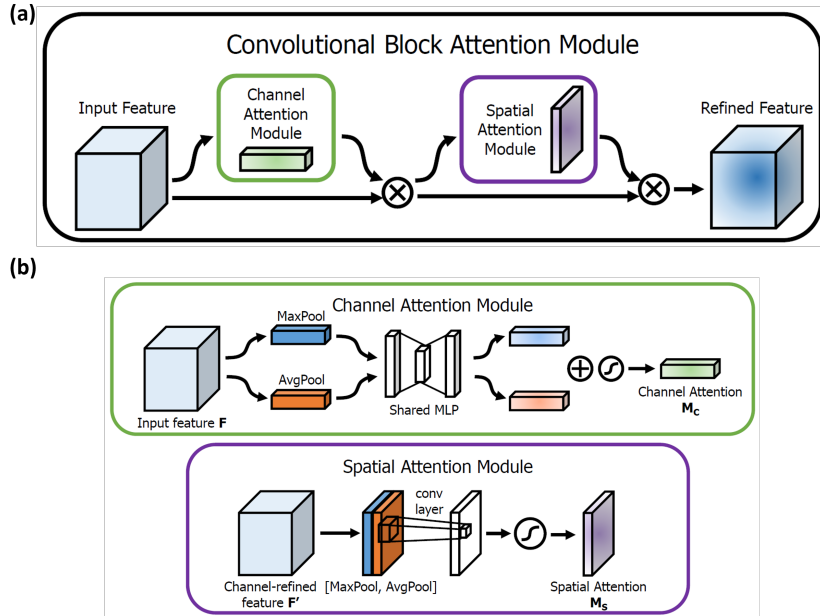


Figure 8: The convolutional block attention module architecture (CBAM)(a) and the channel attention and spatial attention sub-modules(b).

2.4.3. Model validation

To evaluate our model, four common metrics were used: accuracy (A), precision (P), recall (R), and F1-score (F). These metrics rely on values obtained from the confusion matrix, where true-positive (TP) and true-negative (TN) signify correctly predicted positive and negative samples, while false-positive (FP)

and false-negative (FN) represent misclassified positive and negative samples. The calculations for these metrics are as follows:

$$A = \frac{TP + TN}{TP + FP + TN + FN} \quad (7)$$

$$P = \frac{TP}{TP + FP} \quad (8)$$

$$R = \frac{TP}{TP + FN} \quad (9)$$

$$F = \frac{2PR}{P + R} \quad (10)$$

Additionally, the evaluation incorporated the use of the receiver operating characteristic (ROC) curve and the area under the curve (AUC). The ROC curve plots "1-specificity" on the X-axis against "sensitivity" on the Y-axis. Specifically, false positive rate (FPR) is represented by "1-specificity", and true positive rate (TPR) is represented by "sensitivity". These measures are computed as follows:

$$FPR = \frac{FN}{FN + TP} \quad (11)$$

$$TPR = \frac{TP}{TP + FN} \quad (12)$$

The AUC value ranges from 0.5 to 1. A higher AUC means better classification performance.

2.4.4. Sensitivity analysis

Sensitivity analysis offers a comprehensive approach to assess the impact of variables or parameters on the variability and uncertainty within numerical model outputs (Xing et al. 2021). Widely adopted for statistical assessments of model characteristics, the Jackknife test holds particular significance, especially in the context of AUC-based statistical coefficients, and is recognized for its effectiveness in addressing a diverse array of practical challenges (Bandos et al. 2017). Hence, in our study, the Jackknife test was used to evaluate the sensitivity of a specific factor to flash flooding.

In this test, we compared predictions based on all dependent variables with predictions deliberately excluding one dependent variable. Our focus was on observing the resultant reduction in AUC concerning the original value (Park 2015). The percentage of relative decrease (PRD) emerged as a crucial metric in this analysis. The importance of the excluded factor is considered more pronounced if the PRD experiences a more substantial reduction. The PRD is determined by the formula:

$$PRD_i = \frac{100 \times |AUC_o - AUC_i|}{AUC_o} \quad (13)$$

Here, AUC_o represents the original AUC value encompassing all factors, while AUC_i denotes the AUC value when the i -th factor has been excluded.

3. Results

3.1. Factor optimization

The correlation between flash flood predictors was calculated using the Pearson coefficient, as shown in Figure 9. The results indicate that most variables have a low correlation, suggesting they are independent. However, a slightly moderate correlation appears between landcover and elevation, slope and rainfall, NDVI and landcover, as well as distance to stream and drainage density. This correlation is not significant. The multi-collinearity analysis was conducted using the VIF to enhance the prediction power and performance of the model. The results are summarized in Table 2. The VIF values range from 1.0086 to 4.7282, with rainfall exhibiting the highest value and aspect the lowest. These findings imply that there are no multi-collinearity problems among the flash flood variables. Therefore, all 16 variables were included in the present study.

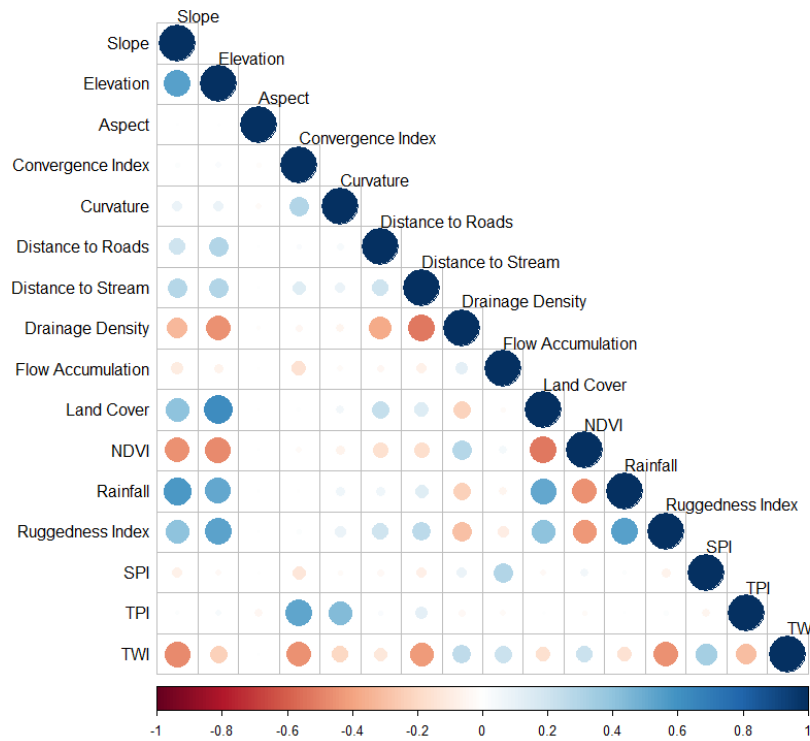


Figure 9: Pearson's correlation analysis between the conditioning factors. SPI: Stream power index, TPI: Topographic positioning index, TWI: Topographic wetness index.

Table 2: Multi-collinearity analysis (VIF) result

Variable	VIF
Elevation	4.4922
Slope	4.5012
Aspect	1.0086
Convergence index	1.8449
Curvature	1.2732
Distance to roads	1.3563
Distance to stream	1.6339
Drainage Density	1.8492
Flow accumulation	1.2999
Land cover	2.6179
NDVI	2.7874
Rainfall	4.7282
Ruggedness index	2.6248
SPI	1.3935
TPI	1.7260
TWI	2.4336

3.2. Model validation

The performance of the twelve models was assessed using various standard quantitative metrics (Table 3). The results show that adding the CBAM attention module significantly improved performance, demonstrating its effectiveness in flash flood susceptibility modeling. In addition, the location of the CBAM block within the backbone architectures influenced accuracy, with embedding CBAM in each convolutional block yielding the best results. Among the models, DenseNet+CBAM-In achieved the highest accuracy (1 and 0.95), followed by Xception+CBAM-In, ResNet+CBAM-In, Xception+CBAM-Tail, Xception+CBAM-Head, DenseNet+CBAM-Tail, ResNet+CBAM-Head, DenseNet+CBAM-Head, ResNet+CBAM-Tail, ResNet, DenseNet, and Xception. The DenseNet+CBAM-In model also excelled in precision, recall, and F1-score metrics, indicating its ability for creating more accurate flash flood susceptibility maps.

Table 3: The performance of CNN models with and without the CBAM attention module

Performance metric	ResNet18				DenseNet121				Xception				
	Base	+CBAM-In	+CBAM-Head	+CBAM-Tail	Base	+CBAM-In	+CBAM-Head	+CBAM-Tail	Base	+CBAM-In	+CBAM-Head	+CBAM-Tail	
Training set													
Accuracy	1	1	1	1	1	1	1	1	0.97	1	1	1	0.99
Precision	1	1	1	1	1	1	1	0.99	0.98	1	1	1	0.99
Recall	1	1	1	1	1	1	1	0.99	0.98	1	1	1	0.99
F1-score	1	1	1	1	1	1	1	0.99	0.98	1	1	1	0.99
Testing set													
Accuracy	0.86	0.92	0.89	0.87	0.85	0.95	0.88	0.9	0.83	0.93	0.9	0.9	0.92
Precision	0.87	0.92	0.89	0.88	0.91	0.95	0.88	0.9	0.82	0.93	0.91	0.91	0.92
Recall	0.87	0.92	0.89	0.88	0.9	0.95	0.88	0.9	0.82	0.92	0.9	0.9	0.92
F1-score	0.87	0.92	0.89	0.88	0.9	0.95	0.88	0.9	0.82	0.92	0.9	0.9	0.92
Number of parameters													
	575697	598741	575844	584259	7085185	7524609	7085332	7217443	20867273	21604006	20867420	21393835	

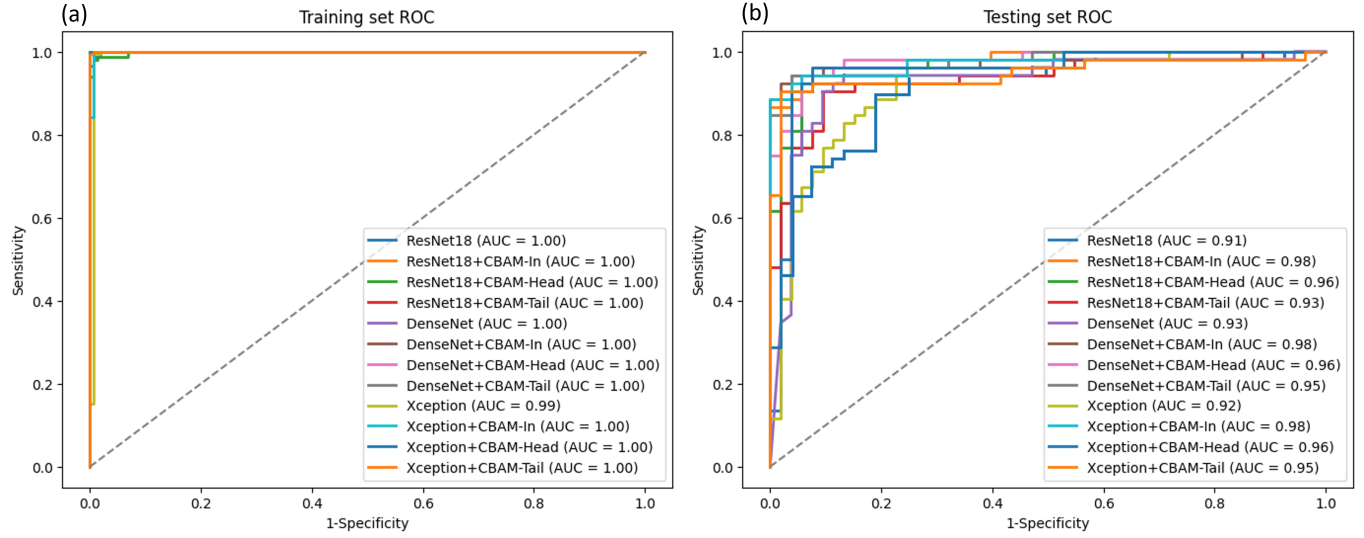


Figure 10: ROC curve and AUC value of the (a) training set and (b) testing set.

According to the ROC results (Figure 10), all models demonstrated very high performance in terms of AUC values on the training sets ($AUC = 1$), except for Xception, which had a slightly lower value ($AUC = 0.99$). On the test sets, the models varied in predictive performance, with AUC values ranging from 0.91 to 0.98. DenseNet+CBAM-In, Xception+CBAM-In, and ResNet+CBAM-In exhibited the highest AUC value of 0.98, while ResNet showed the lowest performance with an AUC of 0.91. In general, all models achieved an outstanding flash flood susceptibility assessment (AUC values surpassing 0.90) (Hosmer et al., 2013). DenseNet+CBAM-In demonstrated superior predictive and generalization capabilities compared with the other models based on all evaluation metrics. Therefore, this model was finally chosen to generate the flash flood susceptibility map of the Rheraya watershed.

3.3. Mapping flash flood susceptibility

Flash flood susceptibility was mapped using the best-performing models (i.e., DenseNet+CBAM-In). The output was categorized into five distinct classes: very low, low, moderate, high, and very high susceptibility, using the natural break classification method (Figure 11). Areas with high and very high flash flood susceptibility are primarily located along rivers, in regions with high drainage density, and concentrated in low-elevation zones. In terms of area proportion, the very high susceptibility class covered only 4.66% of the study area, while the very low and low susceptibility classes were the most dominant, with values of 74.03% and 10.47%, respectively (table 4). These lower susceptibility areas are characterized by high altitudes and significant distance from rivers.

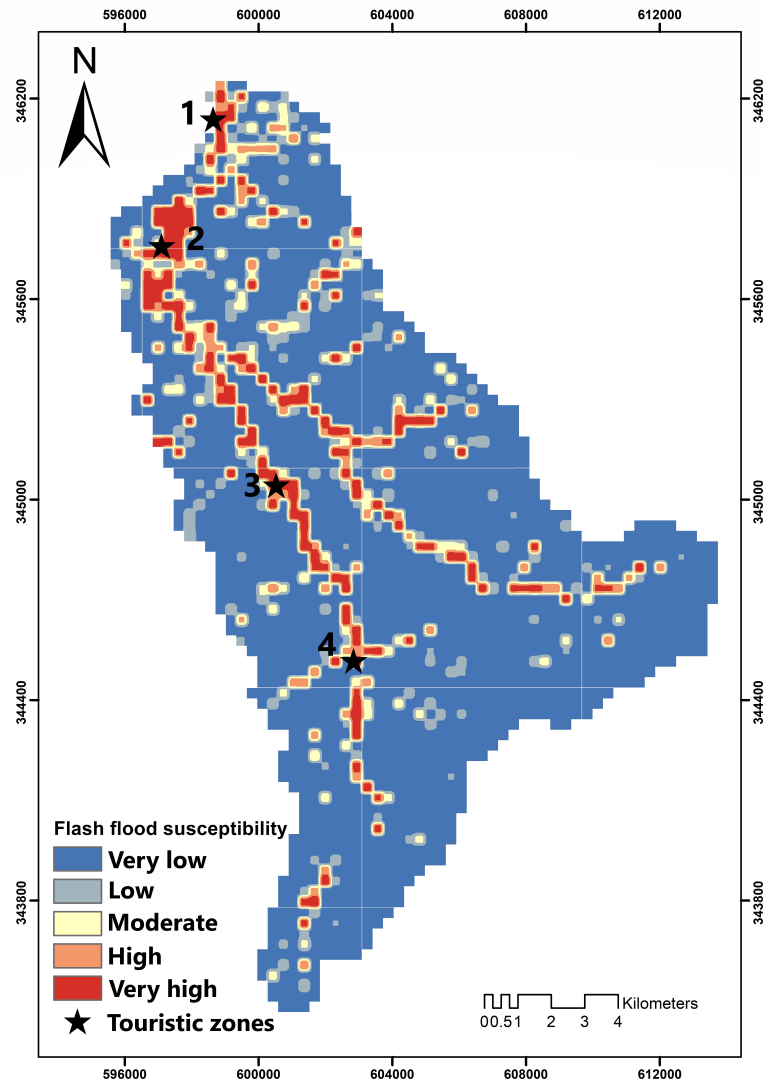


Figure 11: Flash flood susceptibility map of the Rheraya watershed using the DenseNet+CBAM-In model. 1: Moulay Brahim; 2: Asni; 3: Tinine; 4: Imlil

The high and very high susceptibility to flash floods in the study area is notably concentrated in touristic zones such as Moulay Brahim, Asni, Imlil, and Tinitine. Therefore, these regions require significant attention from decision-makers to implement robust flood risk management strategies. To further validate our results, we assessed the distribution of flash flood events across each susceptibility zone (table 4). The distribution of these flash flood events across different susceptibility classes confirms the validity of the susceptibility assessment results (Zhongping et al. 2020). The results show that almost 73% of historical flash flood events were in high and very high susceptibility areas, with very few events in very low susceptibility areas. This

Table 4: Distribution of flash flood susceptibility areas and the proportion of different flash flood events across susceptibility classes.

Class	Percentage of flash flood susceptible areas (%)	Proportion of different flash flood events (%)
Very low	74.03	3.15
Low	10.47	4.33
Moderate	6.28	18.90
High	4.56	20.87
Very high	4.66	52.76

indicates that the DenseNet+CBAM-In model effectively and reliably identified the link between historical flash flood events and flash flood-related variables, accurately pinpointing high susceptibility zones.

3.4. Sensitivity analysis

The Jackknife test method was used to analyze the sensitivity of 16 factors related to flash flooding. The findings indicate that the distance to streams and drainage density have the most significant impact on flash floods in the Rheraya watershed, showing very high sensitivity ($PRD > 0.20$) compared to other factors (Figure 12). Elevation, slope, NDVI, and TPI also demonstrate high sensitivity, with PRD values around 0.18. Other factors such as TWI, SPI, rainfall, landcover, aspect, flow accumulation, distance to roads, and curvature demonstrate a moderate influence on flash floods ($0.07 < PRD < 0.12$). In contrast, the ruggedness index and convergence index show the lowest sensitivity values ($PRD = 0.04$), suggesting they have little contribution to flash flood susceptibility in the study area.

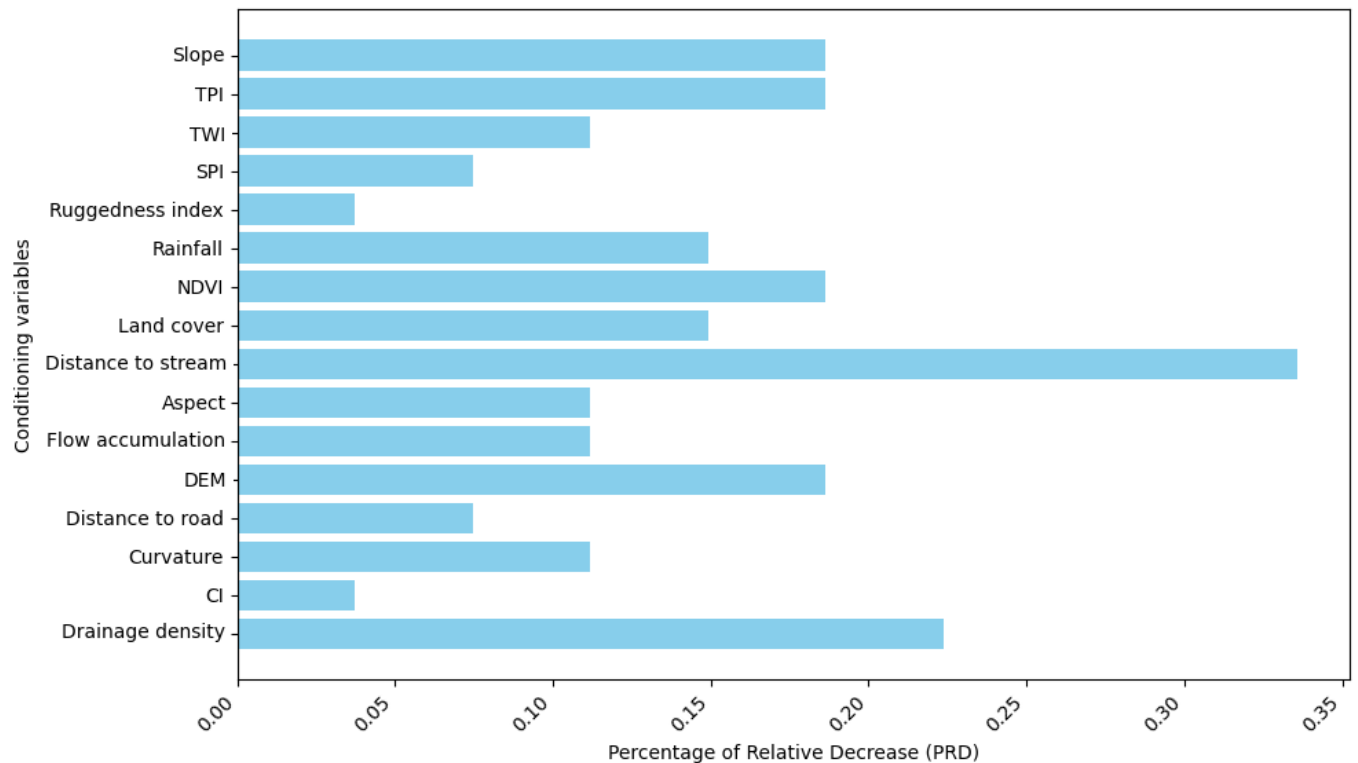


Figure 12: Sensitivity analysis results. TPI: Topographic position index; TWI: Topographic wetness index; SPI: Stream power index; CI: Convergence index.

4. Discussion

To effectively prevent and mitigate flood hazards, it is essential to adopt suitable flood modeling techniques. Thus, exploring new and robust methods for assessing flash flood susceptibility is crucial. In this study, we present an attention-based deep learning model to assess flash flood susceptibility in the Rheraya watershed, a flood-prone region. We compared its performance with state-of-the-art baseline CNN architectures, such as ResNet18, DenseNet121, and Xception. We showed that integrating the CBAM block into the CNN architecture significantly improves model performance. In addition, we demonstrated that the location of the CBAM attention module within the architecture significantly influences the performance of the flash flood susceptibility models. To the best of our knowledge, this is the first study to apply attention-based deep learning to flash flood susceptibility and assess the impact of the attention-block module’s location within the architecture on flash flood susceptibility model performance.

In recent years, artificial intelligence has advanced significantly in flood susceptibility modeling, with traditional machine learning methods like RF, KNN, and SVM being effectively employed to identify highly flood-prone areas (Abu El-Magd 2022; El-Magd et al. 2021; Tehrani et al. 2015). However, deep learning techniques, particularly CNNs, have shown superior performance in automatically extracting high-throughput features for flood susceptibility mapping (Bui et al. 2020a; Costache et al. 2020b; Shahabi et al.

2021; Tsangaratos et al. 2023; Yang et al. 2022). Despite their robustness, CNNs still suffer from drawbacks, such as gradient explosion or vanishing in deeper networks and overfitting in wider ones (Joshi et al. 2019). To mitigate these challenges, our study incorporated an attention module, specifically CBAM, into various deep learning networks, aiming to enhance effective feature weighting and reduce invalid weight features. Our results indicate that attention-based CNNs consistently outperform CNNs without an attention mechanism. This was also shown by Mao et al. (2023) and Ravi & Alazab (2023), where authors showed that attention-based CNNs outperformed non-attention-based CNNs in distinguishing benign from malignant breast lesions and in malware classification, respectively. Similarly, Alirezazadeh et al. (2023) compared the performance of multiple well-known CNN architectures, such as EfficientNetB0, MobileNetV2, ResNet50, InceptionV3, and VGG19, with and without the convolutional block attention module (CBAM) for plant disease classification and showed that EfficientNetB0+CBAM has outperformed all the other models. In addition, we evaluated the impact of CBAM placement within CNN architectures, comparing its integration in each convolutional block, in the head, and in the tail of the CNN architectures. The findings demonstrate that models integrating the CBAM block in each convolutional block yielded the highest accuracy and AUC values compared to those with CBAM only tailing or heading the architecture. For the best performing model, DenseNet121 integrated with CBAM in each convolutional block outperforms all the other models in flash flood susceptibility modeling in terms of accuracy, precision, recall, F1-score, and AUC values. It achieved an accuracy of 0.95 and an AUC value of 0.98, followed by Xception+CBAM-In (accuracy= 0.93; AUC= 0.98), ResNet+CBAM-In (accuracy= 0.92; AUC= 0.98), Xception+CBAM-Tail (accuracy= 0.92; AUC= 0.95), Xception+CBAM-Head (accuracy= 0.9; AUC= 0.96), DenseNet+CBAM-Tail (accuracy=0.9; AUC= 0.96), ResNet+CBAM-Head (accuracy= 0.89; AUC= 0.96), DenseNet+CBAM-Head (accuracy= 0.88; AUC= 0.95), and ResNet+CBAM-Tail (accuracy= 0.87; AUC= 0.93). In summary, our study demonstrated that integrating the CBAM attention module into each convolutional block significantly enhances the accuracy and reliability of CNNs for flash flood susceptibility modeling, highlighting the module’s broad applicability and effectiveness across various architectures.

The sensitivity analysis identified several key factors affecting flash flood susceptibility in the Rheraya watershed, including elevation, slope, distance to streams, NDVI, TPI, rainfall, and drainage density. This underscores the intricate nature of flash floods, which arise from the interplay of topographical features, land use characteristics, and hydrological conditions. Determining the most significant contributor to flash floods in our area is crucial for implementing focused and efficient mitigation strategies, allocating resources wisely, and accurately assessing risks. The distance to streams was found to be the most influential factor in this context. This is consistent with the results of Elghouat et al. (2024), where the authors highlighted that the distance to river and the drainage density were the most influencing factors in flash floods in the Rheraya watershed. Numerous studies have also validated the significant role of these factors in flood occurrence (Rahmati et al. 2016; Pham et al. 2020; Bansal et al. 2022; Chaulagain et al. 2023). This is because areas close to riverbanks are more vulnerable due to their higher exposure to swift water flow and their function as

natural drainage paths. Concerning the resulting flash flood susceptibility map, it indicates that areas at low elevations, with high drainage density, and situated along the river network are particularly prone to flash floods. The Rheraya watershed, known for its scenic landscapes and popular tourist destinations (El Fels et al. 2018), shows a significant portion of these tourist areas, such as Moulay Brahim, Asni, Tinitine, and Imlil, as highly vulnerable to flash floods. These regions urgently require enhanced disaster preparedness and mitigation efforts. Strengthening disaster management infrastructure in these locations is crucial, including the installation of additional meteorological stations to improve rainfall measurement and flood forecasting capabilities. In addition, urban development regulations must be enforced to ensure that new construction is flood-resistant and not located in high-risk zones, particularly near riverbanks.

While this research highlighted the efficacy of attention-based CNNs for pinpointing high-susceptible flash flood zones in the ungauged Rheraya watershed, it has certain limitations. Our analysis was confined to attention-based CNNs and baseline CNN architectures, which restricted the generalizability of our results. In future work, other deep learning models such as transformers and graph neural networks, in addition to the common machine learning algorithms, should also be included in the comparison to further assess and validate our approach. The selection of flash flood factors is also crucial in susceptibility assessment. Using an optimal number of conditioning variables is vital, as an excessive number of features can significantly impact the model’s performance (Pham et al. 2021). Future work could consider leveraging additional data sources and validating models under varied conditions to improve flash flood susceptibility mapping accuracy. Climate models, for instance, could provide data for different future scenarios, which could enhance flash flood susceptibility maps. Furthermore, collaborative data collection and sharing efforts could improve data availability, ranging from local to global flood inventories, enabling model performance evaluations across diverse spatial scales and testing their adaptability and generalizability. The severity of flash floods is greatly influenced by rainfall characteristics (Saharia et al. 2021). Thus, future studies should also consider incorporating rainfall-related factors like intensity, duration, spatial distribution, and temporal patterns into the models. Moreover, the frequency of floods is a crucial factor for flash flood susceptibility (Zhou et al. 2019), yet it appears to be underrepresented in flood-related machine learning and deep learning approaches. Finally, our study’s reliance on data from a single site limits the generalizability of our findings to other ungauged basins. To ensure the scalability and robustness of our approach, it is imperative to evaluate the accuracy of our method across basins with different geo-environmental settings.

5. Conclusion

Developing accurate flash flood susceptibility maps with advanced modeling approaches is crucial for protecting communities, planning infrastructure, and mitigating risks. In this study, we investigated the convolutional block attention module (CBAM) to enhance the performance of CNN networks for flash flood susceptibility modeling by integrating it into baseline architectures such as ResNet18, DenseNet121, and Xception and assessed their performance with and without the attention module. We also evaluated the

influence of the attention module's location within the architecture by integrating it at the head, tail, and within each convolutional block of the backbone architecture. Sixteen flash flood conditioning factors and 522 flash flood inventory points were used as inputs for the modeling. We demonstrated that the attention-based approach outperformed non-attention-based CNNs in flash flood susceptibility modeling, with the best results achieved by integrating the attention module within each convolutional block of the backbone architecture. The best-performing model, the attention-based DenseNet121, achieved an accuracy of 0.95 and an AUC value of 0.98 on the test set, indicating the robustness and generalizability of our approach for accurately identifying the relationship between conditioning factors and flash flood occurrence. Sensitivity analysis revealed that distance to river and drainage density are the most influential factors in flash flood susceptibility. Our maps indicate that highly touristic zones such as Moulay Brahim, Asni, Imlil, and Tinine are highly susceptible to flash floods, consistent with previous studies in the Rheraya watershed. Our analysis was limited to attention-based CNNs and baseline architectures, future work should include other deep learning models like transformers and graph neural networks, as well as traditional machine learning algorithms, to further validate the generalizability of our approach. Additionally, leveraging more data sources and validating models under varied conditions can improve mapping accuracy. Overall, our approach can provide valuable support for policymakers in planning and managing flash flood risks in ungauged basins with high-traffic areas.

Declaration of Competing Interest

The authors declare that they have no known competing financial interests or personal relationships that could have appeared to influence the work reported in this paper.

Data availability

The dataset generated during and/or analyzed during the current study is available from the corresponding author on reasonable request.

Code availability

The scripts used to perform this study will be made available to the public after the acceptance of the paper.

References

Abdel Hamid, H., Wenlong, W., & Qiaomin, L. (2020). Environmental sensitivity of flash flood hazard using geospatial techniques. *Global Journal of Environmental Science and Management*, 6, 31–46.

- Abu El-Magd, S. A. (2022). Random forest and naïve bayes approaches as tools for flash flood hazard susceptibility prediction, south ras el-zait, gulf of suez coast, egypt. *Arabian Journal of Geosciences*, *15*, 217.
- Ahmed, K. R., & Akter, S. (2017). Analysis of landcover change in southwest bengal delta due to floods by ndvi, ndwi and k-means cluster with landsat multi-spectral surface reflectance satellite data. *Remote Sensing Applications: Society and Environment*, *8*, 168–181.
- Alam, A., Ahmed, B., & Sammonds, P. (2021). Flash flood susceptibility assessment using the parameters of drainage basin morphometry in se bangladesh. *Quaternary International*, *575*, 295–307.
- Alirezazadeh, P., Schirrmann, M., & Stolzenburg, F. (2023). Improving deep learning-based plant disease classification with attention mechanism. *Gesunde Pflanzen*, *75*, 49–59.
- Alzubaidi, L., Zhang, J., Humaidi, A. J., Al-Dujaili, A., Duan, Y., Al-Shamma, O., Santamaría, J., Fadhel, M. A., Al-Amidie, M., & Farhan, L. (2021). Review of deep learning: Concepts, cnn architectures, challenges, applications, future directions. *Journal of big Data*, *8*, 1–74.
- Bandos, A. I., Guo, B., & Gur, D. (2017). Jackknife variance of the partial area under the empirical receiver operating characteristic curve. *Statistical methods in medical research*, *26*, 528–541.
- Bansal, N., Mukherjee, M., & Gairola, A. (2022). Evaluating urban flood hazard index (ufhi) of dehradun city using gis and multi-criteria decision analysis. *Modeling earth systems and environment*, (pp. 1–14).
- Benito, G., Rico, M., Sánchez-Moya, Y., Sopeña, A., Thorndycraft, V., & Barriendos, M. (2010). The impact of late holocene climatic variability and land use change on the flood hydrology of the guadalestín river, southeast spain. *Global and Planetary Change*, *70*, 53–63.
- Bentivoglio, R., Isufi, E., Jonkman, S. N., & Taormina, R. (2022). Deep learning methods for flood mapping: a review of existing applications and future research directions. *Hydrology and Earth System Sciences*, *26*, 4345–4378.
- Beven, K. J., & Kirkby, M. J. (1979). A physically based, variable contributing area model of basin hydrology/un modèle à base physique de zone d’appel variable de l’hydrologie du bassin versant. *Hydrological sciences journal*, *24*, 43–69.
- Boudhar, A., Duchemin, B., Hanich, L., Chaponnière, A., Maisongrande, P., Boulet, G., Stitou, J., & Chehbouni, G. (2007). Analyse de la dynamique des surfaces enneigées du haut atlas marocain à partir des données spot-vegetation. *Science et changements planétaires/Sécheresse*, *18*, 278–288.
- Bouwer, L. M., Bubeck, P., & Aerts, J. C. (2010). Changes in future flood risk due to climate and development in a dutch polder area. *Global Environmental Change*, *20*, 463–471.

- Bui, D. T., Hoang, N.-D., Martínez-Álvarez, F., Ngo, P.-T. T., Hoa, P. V., Pham, T. D., Samui, P., & Costache, R. (2020a). A novel deep learning neural network approach for predicting flash flood susceptibility: A case study at a high frequency tropical storm area. *Science of The Total Environment*, *701*, 134413.
- Bui, Q.-T., Nguyen, Q.-H., Nguyen, X. L., Pham, V. D., Nguyen, H. D., & Pham, V.-M. (2020b). Verification of novel integrations of swarm intelligence algorithms into deep learning neural network for flood susceptibility mapping. *Journal of Hydrology*, *581*, 124379.
- Butler, D., Kokkalidou, A., & Makropoulos, C. K. (2006). Supporting the siting of new urban developments for integrated urban water resource management. In *Integrated urban water resources management* (pp. 19–34). Springer.
- Cao, C., Xu, P., Wang, Y., Chen, J., Zheng, L., & Niu, C. (2016). Flash flood hazard susceptibility mapping using frequency ratio and statistical index methods in coalmine subsidence areas. *Sustainability*, *8*, 948.
- Chapi, K., Singh, V. P., Shirzadi, A., Shahabi, H., Bui, D. T., Pham, B. T., & Khosravi, K. (2017). A novel hybrid artificial intelligence approach for flood susceptibility assessment. *Environmental modelling & software*, *95*, 229–245.
- Chaulagain, D., Rimal, P. R., Ngando, S. N., Nsafon, B. E. K., Suh, D., & Huh, J.-S. (2023). Flood susceptibility mapping of kathmandu metropolitan city using gis-based multi-criteria decision analysis. *Ecological Indicators*, *154*, 110653.
- Chen, F., & Tsou, J. Y. (2021). Drsnet: Novel architecture for small patch and low-resolution remote sensing image scene classification. *International Journal of Applied Earth Observation and Geoinformation*, *104*, 102577.
- Chollet, F. (2017). Xception: Deep learning with depthwise separable convolutions. In *Proceedings of the IEEE conference on computer vision and pattern recognition* (pp. 1251–1258).
- Choubin, B., Moradi, E., Golshan, M., Adamowski, J., Sajedi-Hosseini, F., & Mosavi, A. (2019). An ensemble prediction of flood susceptibility using multivariate discriminant analysis, classification and regression trees, and support vector machines. *Science of the Total Environment*, *651*, 2087–2096.
- Chu, H., Wu, W., Wang, Q. J., Nathan, R., & Wei, J. (2020). An ann-based emulation modelling framework for flood inundation modelling: Application, challenges and future directions. *Environmental Modelling & Software*, *124*, 104587.
- Cloke, H. L., & Pappenberger, F. (2009). Ensemble flood forecasting: A review. *Journal of hydrology*, *375*, 613–626.

- Costache, R., Hong, H., & Pham, Q. B. (2020a). Comparative assessment of the flash-flood potential within small mountain catchments using bivariate statistics and their novel hybrid integration with machine learning models. *Science of the Total Environment*, *711*, 134514.
- Costache, R., Ngo, P. T. T., & Bui, D. T. (2020b). Novel ensembles of deep learning neural network and statistical learning for flash-flood susceptibility mapping. *Water*, *12*, 1549.
- Costache, R., Tin, T. T., Arabameri, A., Crăciun, A., Ajin, R., Costache, I., Islam, A. R. M. T., Abba, S., Sahana, M., Avand, M. et al. (2022). Flash-flood hazard using deep learning based on h2o r package and fuzzy-multicriteria decision-making analysis. *Journal of Hydrology*, *609*, 127747.
- Costache, R., & Zaharia, L. (2017). Flash-flood potential assessment and mapping by integrating the weights-of-evidence and frequency ratio statistical methods in gis environment—case study: Bâsca chiojdului river catchment (romania). *Journal of Earth System Science*, *126*, 59.
- Dahri, N., & Abida, H. (2017). Monte carlo simulation-aided analytical hierarchy process (ahp) for flood susceptibility mapping in gabes basin (southeastern tunisia). *Environmental earth sciences*, *76*, 1–14.
- De Leijster, V., Santos, M., Wassen, M., García, J. C., Fernandez, I. L., Verkuil, L., Scheper, A., Steenhuis, M., & Verweij, P. (2021). Ecosystem services trajectories in coffee agroforestry in colombia over 40 years. *Ecosystem Services*, *48*, 101246.
- DeVries, B., Huang, C., Armston, J., Huang, W., Jones, J. W., & Lang, M. W. (2020). Rapid and robust monitoring of flood events using sentinel-1 and landsat data on the google earth engine. *Remote Sensing of Environment*, *240*, 111664.
- DIGBY, B. (2000). *Changing environments*. Heinemann.
- Dodangeh, E., Choubin, B., Eigdir, A. N., Nabipour, N., Panahi, M., Shamsirband, S., & Mosavi, A. (2020). Integrated machine learning methods with resampling algorithms for flood susceptibility prediction. *Science of the Total Environment*, *705*, 135983.
- Eini, M., Kaboli, H. S., Rashidian, M., & Hedayat, H. (2020). Hazard and vulnerability in urban flood risk mapping: Machine learning techniques and considering the role of urban districts. *International Journal of Disaster Risk Reduction*, *50*, 101687.
- El Fels, A. E. A. et al. (2018). Flood frequency analysis and generation of flood hazard indicator maps in a semi-arid environment, case of ourika watershed (western high atlas, morocco). *Journal of African Earth Sciences*, *141*, 94–106.
- El-Magd, S. A. A., Pradhan, B., & Alamri, A. (2021). Machine learning algorithm for flash flood prediction mapping in wadi el-laqeita and surroundings, central eastern desert, egypt. *Arabian Journal of Geosciences*, *14*, 323.

- Elghouat, A., Algouti, A., Algouti, A., Baid, S., Ezzahzi, S., Kabili, S., & Agli, S. (2024). Integrated approaches for flash flood susceptibility mapping: spatial modeling and comparative analysis of statistical and machine learning models. a case study of the rheraya watershed, morocco. *Journal of Water and Climate Change*, (p. jwc2024726).
- Elmore, A. J., Julian, J. P., Guinn, S. M., & Fitzpatrick, M. C. (2013). Potential stream density in mid-atlantic us watersheds. *PLoS One*, *8*, e74819.
- ESRI, R. (2011). Arcgis desktop: release 10. *Environmental Systems Research Institute, CA*, *634*, 315–325.
- Fernández, D., & Lutz, M. A. (2010). Urban flood hazard zoning in tucumán province, argentina, using gis and multicriteria decision analysis. *Engineering Geology*, *111*, 90–98.
- Ginesta Torcivia, C. E., & Ríos López, N. N. (2020). Preliminary morphometric analysis: Río talacasto basin, central precordillera of san juan, argentina. In *Advances in Geomorphology and Quaternary Studies in Argentina: Special Symposium from the Argentine Association of Geomorphology and Quaternary Studies, October 2017* (pp. 158–168). Springer.
- Gudiyangada Nachappa, T., & Meena, S. R. (2020). A novel per pixel and object-based ensemble approach for flood susceptibility mapping. *Geomatics, Natural Hazards and Risk*, *11*, 2147–2175.
- Guerriero, L., Ruzza, G., Guadagno, F. M., & Revellino, P. (2020). Flood hazard mapping incorporating multiple probability models. *Journal of Hydrology*, *587*, 125020.
- Guha-Sapir, D., Below, R., & Hoyois, P. (2016). Em-dat: the cred/ofda international disaster database, .
- Gui, J., Pérez-Rey, I., Yao, M., Zhao, F., & Chen, W. (2023). Credal-decision-tree-based ensembles for spatial prediction of landslides. *Water*, *15*, 605.
- Hayashi, Y. (2019). The right direction needed to develop white-box deep learning in radiology, pathology, and ophthalmology: A short review. *Frontiers in Robotics and AI*, *6*, 24.
- He, K., Zhang, X., Ren, S., & Sun, J. (2016). Deep residual learning for image recognition. In *Proceedings of the IEEE conference on computer vision and pattern recognition* (pp. 770–778).
- Hirabayashi, Y., Mahendran, R., Koirala, S., Konoshima, L., Yamazaki, D., Watanabe, S., Kim, H., & Kanae, S. (2013). Global flood risk under climate change. *Nature climate change*, *3*, 816–821.
- Hong, H., Tsangaratos, P., Ilia, I., Liu, J., Zhu, A.-X., & Chen, W. (2018). Application of fuzzy weight of evidence and data mining techniques in construction of flood susceptibility map of poyang county, china. *Science of the total environment*, *625*, 575–588.
- Hoque, M. A.-A., Tasfia, S., Ahmed, N., & Pradhan, B. (2019). Assessing spatial flood vulnerability at kalapara upazila in bangladesh using an analytic hierarchy process. *Sensors*, *19*, 1302.

- Huang, G., Liu, Z., Van Der Maaten, L., & Weinberger, K. Q. (2017). Densely connected convolutional networks. In *Proceedings of the IEEE conference on computer vision and pattern recognition* (pp. 4700–4708).
- Islam, A. R. M. T., Talukdar, S., Mahato, S., Kundu, S., Eibek, K. U., Pham, Q. B., Kuriqi, A., & Linh, N. T. T. (2021). Flood susceptibility modelling using advanced ensemble machine learning models. *Geoscience Frontiers*, *12*, 101075.
- Jacinto, R., Grosso, N., Reis, E., Dias, L., Santos, F., & Garrett, P. (2015). Continental portuguese territory flood susceptibility index–contribution to a vulnerability index. *Natural Hazards and Earth System Science*, *15*, 1907–1919.
- Jamali, B., Bach, P. M., & Deletic, A. (2020). Rainwater harvesting for urban flood management–an integrated modelling framework. *Water research*, *171*, 115372.
- Jeyaseelan, A. (2003). Droughts & floods assessment and monitoring using remote sensing and gis. *Satellite remote sensing and GIS applications in agricultural meteorology*, 291.
- Joshi, S., Verma, D. K., Saxena, G., & Paraye, A. (2019). Issues in training a convolutional neural network model for image classification. In *Advances in Computing and Data Sciences: Third International Conference, ICACDS 2019, Ghaziabad, India, April 12–13, 2019, Revised Selected Papers, Part II 3* (pp. 282–293). Springer.
- Kabir, S., Patidar, S., Xia, X., Liang, Q., Neal, J., & Pender, G. (2020). A deep convolutional neural network model for rapid prediction of fluvial flood inundation. *Journal of Hydrology*, *590*, 125481.
- Karlsson, C. S., Kalantari, Z., Mörtberg, U., Olofsson, B., & Lyon, S. W. (2017). Natural hazard susceptibility assessment for road planning using spatial multi-criteria analysis. *Environmental management*, *60*, 823–851.
- Khalil, U., Khan, N. M. et al. (2017). Floodplain mapping for indus river: Chashma–taunsa reach. *Pakistan Journal of Engineering and Applied Sciences*, .
- Khoirunisa, N., Ku, C.-Y., & Liu, C.-Y. (2021). A gis-based artificial neural network model for flood susceptibility assessment. *International Journal of Environmental Research and Public Health*, *18*, 1072.
- Khosravi, K., Pham, B. T., Chapi, K., Shirzadi, A., Shahabi, H., Revhaug, I., Prakash, I., & Bui, D. T. (2018). A comparative assessment of decision trees algorithms for flash flood susceptibility modeling at haraz watershed, northern iran. *Science of the Total Environment*, *627*, 744–755.
- Kim, J. H. (2019). Multicollinearity and misleading statistical results. *Korean journal of anesthesiology*, *72*, 558–569.

- Klipalo, E., Besharat, M., & Kuriqi, A. (2022). Full-scale interface friction testing of geotextile-based flood defence structures. *Buildings*, *12*, 990.
- Knighton, A. D. (1999). Downstream variation in stream power. *Geomorphology*, *29*, 293–306.
- Kuenzer, C., Guo, H., Huth, J., Leinenkugel, P., Li, X., & Dech, S. (2013). Flood mapping and flood dynamics of the mekong delta: Envisat-asar-wsm based time series analyses. *Remote Sensing*, *5*, 687–715.
- Kumar, R., & Acharya, P. (2016). Flood hazard and risk assessment of 2014 floods in kashmir valley: a space-based multisensor approach. *Natural Hazards*, *84*, 437–464.
- Li, W., Lin, K., Zhao, T., Lan, T., Chen, X., Du, H., & Chen, H. (2019). Risk assessment and sensitivity analysis of flash floods in ungauged basins using coupled hydrologic and hydrodynamic models. *Journal of Hydrology*, *572*, 108–120.
- Lin, J., He, P., Yang, L., He, X., Lu, S., & Liu, D. (2022). Predicting future urban waterlogging-prone areas by coupling the maximum entropy and flus model. *Sustainable Cities and Society*, *80*, 103812.
- Liu, J., Wang, J., Xiong, J., Cheng, W., Sun, H., Yong, Z., & Wang, N. (2021). Hybrid models incorporating bivariate statistics and machine learning methods for flash flood susceptibility assessment based on remote sensing datasets. *Remote Sensing*, *13*, 4945.
- Mackay, A. (2008). Climate change 2007: impacts, adaptation and vulnerability. contribution of working group ii to the fourth assessment report of the intergovernmental panel on climate change. *Journal of Environmental Quality*, *37*, 2407.
- Mao, N., Zhang, H., Dai, Y., Li, Q., Lin, F., Gao, J., Zheng, T., Zhao, F., Xie, H., Xu, C. et al. (2023). Attention-based deep learning for breast lesions classification on contrast enhanced spectral mammography: a multicentre study. *British Journal of Cancer*, *128*, 793–804.
- Mehmood, H., Conway, C., & Perera, D. (2021). Mapping of flood areas using landsat with google earth engine cloud platform. *Atmosphere*, *12*, 866.
- Mekonnen, M. M., & Hoekstra, A. Y. (2016). Four billion people facing severe water scarcity. *Science advances*, *2*, e1500323.
- Mohanty, M. P., Mudgil, S., & Karmakar, S. (2020). Flood management in india: A focussed review on the current status and future challenges. *International Journal of Disaster Risk Reduction*, *49*, 101660.
- Moore, I. D., Grayson, R., & Ladson, A. (1991). Digital terrain modelling: a review of hydrological, geomorphological, and biological applications. *Hydrological processes*, *5*, 3–30.
- Musolino, G., Ahmadian, R., & Falconer, R. (2020). Comparison of flood hazard assessment criteria for pedestrians with a refined mechanics-based method. *Journal of Hydrology X*, *9*, 100067.

- Nachappa, T. G., Piralilou, S. T., Gholamnia, K., Ghorbanzadeh, O., Rahmati, O., & Blaschke, T. (2020). Flood susceptibility mapping with machine learning, multi-criteria decision analysis and ensemble using dempster shafer theory. *Journal of hydrology*, *590*, 125275.
- Newman, D., Lindsay, J., & Cockburn, J. (2018). Evaluating metrics of local topographic position for multiscale geomorphometric analysis. *Geomorphology*, *312*, 40–50.
- Ngo, P.-T. T., Hoang, N.-D., Pradhan, B., Nguyen, Q. K., Tran, X. T., Nguyen, Q. M., Nguyen, V. N., Samui, P., & Tien Bui, D. (2018). A novel hybrid swarm optimized multilayer neural network for spatial prediction of flash floods in tropical areas using sentinel-1 sar imagery and geospatial data. *Sensors*, *18*, 3704.
- Nguyen, V.-N., Yariyan, P., Amiri, M., Dang Tran, A., Pham, T. D., Do, M. P., Thi Ngo, P. T., Nhu, V.-H., Quoc Long, N., & Tien Bui, D. (2020). A new modeling approach for spatial prediction of flash flood with biogeography optimized chaid tree ensemble and remote sensing data. *Remote Sensing*, *12*, 1373.
- Nhu, V.-H., Thi Ngo, P.-T., Pham, T. D., Dou, J., Song, X., Hoang, N.-D., Tran, D. A., Cao, D. P., Aydilek, I. B., Amiri, M. et al. (2020). A new hybrid firefly–pso optimized random subspace tree intelligence for torrential rainfall-induced flash flood susceptible mapping. *Remote Sensing*, *12*, 2688.
- Nogueira, K., Fadel, S. G., Dourado, Í. C., Werneck, R. d. O., Muñoz, J. A., Penatti, O. A., Calumby, R. T., Li, L. T., dos Santos, J. A., & Torres, R. d. S. (2018). Exploiting convnet diversity for flooding identification. *IEEE Geoscience and Remote Sensing Letters*, *15*, 1446–1450.
- Ongdas, N., Akiyanova, F., Karakulov, Y., Muratbayeva, A., & Zinabdin, N. (2020). Application of hec-ras (2d) for flood hazard maps generation for yesil (ishim) river in kazakhstan. *Water*, *12*, 2672.
- Pamučar, D., Mihajlović, M., Obradović, R., & Atanasković, P. (2017). Novel approach to group multi-criteria decision making based on interval rough numbers: Hybrid dematel-anp-mairca model. *Expert systems with applications*, *88*, 58–80.
- Park, N.-W. (2015). Using maximum entropy modeling for landslide susceptibility mapping with multiple geoenvironmental data sets. *Environmental Earth Sciences*, *73*, 937–949.
- Pham, B., Avand, M., Janizadeh, S., Phong, T., Al-Ansari, N., Ho, L., Das, S., Le, H., Amini, A., Bozchaloei, S. et al. (2020). Gis based hybrid computational approaches for flash flood susceptibility assessment. *water* *12* (3): 683.
- Pham, B. T., Luu, C., Van Dao, D., Van Phong, T., Nguyen, H. D., Van Le, H., von Meding, J., & Prakash, I. (2021). Flood risk assessment using deep learning integrated with multi-criteria decision analysis. *Knowledge-based systems*, *219*, 106899.

- Pourghasemi, H. R., Razavi-Termeh, S. V., Kariminejad, N., Hong, H., & Chen, W. (2020). An assessment of metaheuristic approaches for flood assessment. *Journal of Hydrology*, *582*, 124536.
- Pradhan, B., Lee, S., Dikshit, A., & Kim, H. (2023). Spatial flood susceptibility mapping using an explainable artificial intelligence (xai) model. *Geoscience Frontiers*, *14*, 101625.
- Priscillia, S., Schillaci, C., & Lipani, A. (2021). Flood susceptibility assessment using artificial neural networks in indonesia. *Artificial Intelligence in Geosciences*, *2*, 215–222.
- Rahmati, O., Pourghasemi, H. R., & Zeinivand, H. (2016). Flood susceptibility mapping using frequency ratio and weights-of-evidence models in the golastan province, iran. *Geocarto International*, *31*, 42–70.
- Ravi, V., & Alazab, M. (2023). Attention-based convolutional neural network deep learning approach for robust malware classification. *Computational Intelligence*, *39*, 145–168.
- Saha, T. K., Pal, S., Talukdar, S., Debanshi, S., Khatun, R., Singha, P., & Mandal, I. (2021). How far spatial resolution affects the ensemble machine learning based flood susceptibility prediction in data sparse region. *Journal of Environmental Management*, *297*, 113344.
- Sahana, M., Rehman, S., Sajjad, H., & Hong, H. (2020). Exploring effectiveness of frequency ratio and support vector machine models in storm surge flood susceptibility assessment: A study of sundarban biosphere reserve, india. *Catena*, *189*, 104450.
- Saharia, M., Kirstetter, P.-E., Vergara, H., Gourley, J. J., Emmanuel, I., & Andrieu, H. (2021). On the impact of rainfall spatial variability, geomorphology, and climatology on flash floods. *Water resources research*, *57*, e2020WR029124.
- Sedgwick, P. (2012). Pearson’s correlation coefficient. *Bmj*, *345*.
- Shahabi, H., Shirzadi, A., Ronoud, S., Asadi, S., Pham, B. T., Mansouripour, F., Geertsema, M., Clague, J. J., & Bui, D. T. (2021). Flash flood susceptibility mapping using a novel deep learning model based on deep belief network, back propagation and genetic algorithm. *Geoscience Frontiers*, *12*, 101100.
- Stevaux, J. C., de Azevedo Macedo, H., Assine, M. L., & Silva, A. (2020). Changing fluvial styles and back-water flooding along the upper paraguay river plains in the brazilian pantanal wetland. *Geomorphology*, *350*, 106906.
- Tehrany, M. S., Pradhan, B., & Jebur, M. N. (2013). Spatial prediction of flood susceptible areas using rule based decision tree (dt) and a novel ensemble bivariate and multivariate statistical models in gis. *Journal of hydrology*, *504*, 69–79.
- Tehrany, M. S., Pradhan, B., Mansor, S., & Ahmad, N. (2015). Flood susceptibility assessment using gis-based support vector machine model with different kernel types. *Catena*, *125*, 91–101.

- Tingsanchali, T. (2012). Urban flood disaster management. *Procedia engineering*, 32, 25–37.
- Tong, W., Chen, W., Han, W., Li, X., & Wang, L. (2020). Channel-attention-based densenet network for remote sensing image scene classification. *IEEE Journal of Selected Topics in Applied Earth Observations and Remote Sensing*, 13, 4121–4132.
- Tsangaratos, P., Ilia, I., Chrysafi, A.-A., Matiatos, I., Chen, W., & Hong, H. (2023). Applying a 1d convolutional neural network in flood susceptibility assessments—the case of the island of euboea, greece. *Remote Sensing*, 15, 3471.
- Vaswani, A., Shazeer, N., Parmar, N., Uszkoreit, J., Jones, L., Gomez, A. N., Kaiser, Ł., & Polosukhin, I. (2017). Attention is all you need. *Advances in neural information processing systems*, 30.
- Vojtek, M., & Vojteková, J. (2019). Flood susceptibility mapping on a national scale in slovakia using the analytical hierarchy process. *Water*, 11, 364.
- Wang, Y., Fang, Z., Hong, H., & Peng, L. (2020a). Flood susceptibility mapping using convolutional neural network frameworks. *Journal of Hydrology*, 582, 124482.
- Wang, Y., Fang, Z., Wang, M., Peng, L., & Hong, H. (2020b). Comparative study of landslide susceptibility mapping with different recurrent neural networks. *Computers & Geosciences*, 138, 104445.
- Wilson, J. P., & Gallant, J. C. (2000). *Terrain analysis: principles and applications*. John Wiley & Sons.
- Woo, S., Park, J., Lee, J.-Y., & Kweon, I. S. (2018). Cbam: Convolutional block attention module. In *Proceedings of the European conference on computer vision (ECCV)* (pp. 3–19).
- Woodruff, J. D., Irish, J. L., & Camargo, S. J. (2013). Coastal flooding by tropical cyclones and sea-level rise. *Nature*, 504, 44–52.
- Xing, Y., Shao, D., Yang, Y., Ma, X., & Zhang, S. (2021). Influence and interactions of input factors in urban flood inundation modeling: An examination with variance-based global sensitivity analysis. *Journal of Hydrology*, 600, 126524.
- Yang, R., Zheng, G., Hu, P., Liu, Y., Xu, W., & Bao, A. (2022). Snowmelt flood susceptibility assessment in kunlun mountains based on the swin transformer deep learning method. *Remote Sensing*, 14, 6360.
- Young, R. A., & Mutchler, C. K. (1969). Soil movement on irregular slopes. *Water Resources Research*, 5, 1084–1089.
- Zanaga, D., Van De Kerchove, R., Daems, D., De Keersmaecker, W., Brockmann, C., Kirches, G., Wevers, J., Cartus, O., Santoro, M., Fritz, S. et al. (2022). Esa worldcover 10 m 2021 v200, .

- Zeng, Z., Li, Y., Lan, J., & Hamidi, A. R. (2021). Utilizing user-generated content and gis for flood susceptibility modeling in mountainous areas: A case study of jian city in china. *Sustainability*, *13*, 6929.
- Zhang, J., Lu, C., Li, X., Kim, H.-J., & Wang, J. (2019). A full convolutional network based on densenet for remote sensing scene classification. *Mathematical Biosciences and Engineering*, *16*, 3345–3367.
- Zhao, G., Pang, B., Xu, Z., Peng, D., & Zuo, D. (2020). Urban flood susceptibility assessment based on convolutional neural networks. *Journal of Hydrology*, *590*, 125235.
- Zheng, M., Xu, J., Shen, Y., Tian, C., Li, J., Fei, L., Zong, M., & Liu, X. (2022). Attention-based cnns for image classification: A survey. In *Journal of Physics: Conference Series* (p. 012068). IOP Publishing volume 2171.
- Zhongping, Z., Jiangwei, W., & Shangjun, Z. (2020). The susceptibility assessment of flood disaster in mountain cities based on gis and logistic regression analysis: a case study of ji'an city, jiangxi province. *Resources and environment in the Yangtze Basin*. <https://kns.cnki.net/kcms/detail/42.1320.X, 20200805>.
- Zhou, T., Liu, Z., Jin, J., & Hu, H. (2019). Assessing the impacts of univariate and bivariate flood frequency approaches to flood risk accounting for reservoir operation. *Water*, *11*, 475.
- Zwoliński, Z., & Stefańska, E. (2015). Relevance of moving window size in landform classification by tpi. *Geomorphometry for Geosciences*, (pp. 273–277).